A nuclear architecture screen in *Drosophila* identifies Stonewall as a link between chromatin position at the nuclear periphery and germline stem cell fate

Ankita Chavan,[1,2,3,10] Randi Isenhart,[4,5,10] Son C. Nguyen,[4,5] Noor M. Kotb,[6] Jailynn Harke,[4,5] Anna Sintsova,[7] Gulay Ulukaya,[8] Federico Uliana,[1] Caroline Ashiono,[1] Ulrike Kutay,[1] Gianluca Pegoraro,[9] Prashanth Rangan,[6] Eric F. Joyce,[4,5] and Madhav Jagannathan[1,2]

[1]Institute of Biochemistry, Department of Biology, Eidgenössische Technische Hochschule (ETH) Zürich, Zürich 8093, Switzerland; [2]Bringing Materials to Life Consortium, ETH Zürich, Zürich 8093, Switzerland; [3]Life Science Zürich Graduate School, Zürich 8057, Switzerland; [4]Penn Epigenetics Institute, Perelman School of Medicine, University of Pennsylvania, Philadelphia, Pennsylvania 19104, USA; [5]Department of Genetics, Perelman School of Medicine, University of Pennsylvania, Philadelphia, Pennsylvania 19104, USA; [6]Department of Cell, Developmental, and Regenerative Biology, Black Family Stem Cell Institute, Icahn School of Medicine at Mount Sinai, New York, New York 10029, USA; [7]Institute of Microbiology, Department of Biology, ETH Zürich, Zürich 8093, Switzerland; [8]Bioinformatics for Next-Generation Sequencing (BiNGS) Core, Tisch Cancer Institute, Icahn School of Medicine at Mount Sinai, New York, New York 10029, USA; [9]High-Throughput Imaging Facility (HiTIF), National Cancer Institute, National Institutes of Health, Bethesda, Maryland 20892, USA

The association of genomic loci to the nuclear periphery is proposed to facilitate cell type-specific gene repression and influence cell fate decisions. However, the interplay between gene position and expression remains incompletely understood, in part because the proteins that position genomic loci at the nuclear periphery remain unidentified. Here, we used an Oligopaint-based HiDRO screen targeting ~1000 genes to discover novel regulators of nuclear architecture in *Drosophila* cells. We identified the heterochromatin-associated protein Stonewall (Stwl) as a factor promoting perinuclear chromatin positioning. In female germline stem cells (GSCs), Stwl binds and positions chromatin loci, including GSC differentiation genes, at the nuclear periphery. Strikingly, Stwl-dependent perinuclear positioning is associated with transcriptional repression, highlighting a likely mechanism for Stwl's known role in GSC maintenance and ovary homeostasis. Thus, our study identifies perinuclear anchors in *Drosophila* and demonstrates the importance of gene repression at the nuclear periphery for cell fate.

[*Keywords*: nuclear architecture; genome organization; nuclear periphery; heterochromatin; germline stem cell]

Supplemental material is available for this article.

Received December 10, 2023; revised version accepted May 21, 2024.

The distribution of the genome within the interphase nucleus can tune cell-specific gene expression. In both plant and animal cells, dense-staining heterochromatin and repressed tissue-specific genes are typically found near the inner nuclear membrane (INM) (van Steensel and Belmont 2017). In metazoans, an INM-associated network involving the intermediate filament protein lamin and other associated proteins serves as a scaffold for the organization of peripheral chromatin (Ungricht and Kutay 2017). This chromatin, which is associated with the nuclear lamina, is referred to as lamina-associated domains (LADs) and is usually gene-poor, transcriptionally silent, and rich in repressive histone marks (Pickersgill et al. 2006; Guelen et al. 2008; Gerstein et al. 2010; Ikegami et al. 2010). Experiments using LAD-embedded transcriptional reporters (Guelen et al. 2008; Dialynas et al. 2010; Peric-Hupkes et al. 2010; Akhtar et al. 2013) and gene tethering to the nuclear periphery (Finlan et al. 2008; Kumaran and Spector 2008; Reddy et al. 2008) have shown that perinuclear positioning is generally associated with reduced transcriptional output, although exceptions can occur (Kumaran and Spector 2008). Functionally, perinuclear positioning of a locus has been speculated to preserve

[10]These authors contributed equally to this work.
Corresponding authors: madhav.jagannathan@bc.biol.ethz.ch, erjoyce@pennmedicine.upenn.edu

Article published online ahead of print. Article and publication date are online at http://www.genesdev.org/cgi/doi/10.1101/gad.351424.123. Freely available online through the *Genes & Development* Open Access option.

the inactive transcriptional state and stabilize cell-specific gene expression programs (van Steensel and Belmont 2017; Guerreiro and Kind 2019). Consistently, detachment of specific loci from the nuclear periphery in multiple cell types is associated with ectopic gene expression and alterations in cell fate decisions (Shevelyov et al. 2009; Kohwi et al. 2013; Chen et al. 2014; Gonzalez-Sandoval et al. 2015). While the nuclear lamina (Shevelyov et al. 2009; Mattout et al. 2011; Kohwi et al. 2013; Chen et al. 2014), nuclear pore complex (NPC) proteins (Gozalo et al. 2020; Iglesias et al. 2020; Sarkar et al. 2023), and epigenetic modifications (Towbin et al. 2012; Bian et al. 2013; Harr et al. 2015) are known to influence chromatin association to the nuclear periphery, very few chromatin-binding perinuclear anchors have been identified thus far (Zullo et al. 2012; Poleshko et al. 2013; Gonzalez-Sandoval et al. 2015). As a result, the precise relationships between perinuclear positioning, gene expression, and cell fate remain enigmatic.

In this study, we leverage our recently developed HiDRO technology (Park et al. 2023) to conduct an RNAi screen in *Drosophila* cells aimed at identifying perinuclear anchors for heterochromatin. We individually depleted ~1000 genes known to possess characteristic DNA-binding domains or nuclear localization sequences and then measured changes in the spatial positioning of genomic regions located both at the periphery and center of the nucleus. Among our hits, we isolated a significant hit—the heterochromatin-associated MADF-BESS domain-containing protein Stonewall (Stwl) (Clark and McKearin 1996)—as a factor important for the peripheral positioning of LAD-enriched chromatin. MADF-BESS proteins are transcriptional regulators that bind DNA through an N-terminal MADF (Myb-SANT-like in ADF) domain, whereas the C-terminal BESS motif mediates protein–protein interactions (Bhaskar and Courey 2002; Shukla et al. 2014). Previous studies have demonstrated that Stwl has a cell-autonomous function in female germline stem cell (GSC) maintenance (Clark and McKearin 1996; Akiyama 2002; Maines et al. 2007) as well as later stages of oogenesis (Clark and McKearin 1996; Maines et al. 2007; Yi et al. 2009; Zinshteyn and Barbash 2022), likely through gene repression. Notably, Stwl-depleted GSCs are reported to differentiate precociously (as determined by fusome-containing germline cysts) even in the absence of critical differentiation genes (Maines et al. 2007), suggesting that Stwl plays an important role in the balance between GSC self-renewal and differentiation. However, the mechanism by which Stwl fine-tunes this vital regulatory step in GSC fate has remained unclear. Here, we show that Stwl is crucial for perinuclear chromatin positioning in female GSCs. Using RNA sequencing, chromatin profiling, and single-molecule FISH (smFISH), we demonstrate that Stwl promotes repression of canonical GSC differentiation genes such as *benign gonial cell neoplasm* (*bgcn*) by positioning these gene loci at the nuclear periphery. Overall, our HiDRO screen has identified multiple factors regulating nuclear architecture in *Drosophila*. Furthermore, we have pinpointed Stwl as an important factor that links perinuclear chromatin organization to female GSC fate.

Results

Discovery of novel regulators of chromosome positioning

To identify proteins involved in the positioning of chromatin at the nuclear periphery, we performed an RNAi screen using our recently developed HiDRO platform (Park et al. 2023) in *Drosophila* Kc167 cells (Fig. 1A). Specifically, we seeded Kc167 cells onto 384 well plates containing individual dsRNAs in each well and performed high-throughput Oligopaint FISH to mark three 1 Mb genomic regions that span chromosome 2R and contain varying amounts of LADs (referred to as chromosomes 2R-A, 2R-B, and 2R-C) (van Bemmel et al. 2010). In particular, 74% of chromosome 2R-C is designated as LADs in Kc167 cells (Fig. 1B). We also confirmed by high-resolution FISH that this region was in closer proximity to the nuclear periphery compared with chromosome 2R-A and chromosome 2R-B (Fig. 1C). We therefore used the normalized distance between this region and the nuclear periphery as our primary metric for isolating hits.

We performed an RNAi screen in duplicate using a *Drosophila* RNAi Screening Center (DRSC)-curated transcription factor dsRNA sublibrary that targets 966 genes encoding DNA-binding or nuclear-localizing proteins. A total of ~8 million cells was analyzed, which yielded 29 "peripheral" hits that significantly increased the distance between chromosome 2R-C and the nuclear periphery, normalized to the nuclear area (Fig. 1D). In addition to our primary metric, we also calculated peripheral distance for chromosome 2R-A and chromosome 2R-B as well as 13 secondary parameters of genome organization, including the pairwise distance between regions A, B, and C. These involved measurements related to the size and shape of each domain and the nucleus itself, creating a multimodal data set of nuclear organization for all 966 genes analyzed (Supplemental Table S1). Together, this revealed that 11 out of 29 peripheral hits also altered chromosome length, with all 11 causing decreased chromosome length, consistent with peripheral detachment leading to a global change in genome organization (Fig. 1E). Consistent with this notion, dsRNAs that altered both metrics exhibited stronger *z*-scores (Fig. 1F) with a strong correlation between their effect sizes ($r^2 = 0.81$) (Supplemental Fig. S1A). Importantly, this was not solely due to changes in nuclear size, which exhibited a weaker correlation with chromosome repositioning ($r^2 = 0.35$) (Supplemental Fig. S1B). Of course, we also note that several dsRNAs led to changes in either chromosome length or positioning, indicating that these two parameters are not exclusively dependent on one another (Fig. 1E,F).

Stwl localizes to the nuclear periphery in Kc167 cells

We used StringDB (Szklarczyk et al. 2015) to find any known relationships between the peripheral hits and recovered four distinct subgroups, one of which included the MADF-BESS domain-containing proteins Su(var)3-7 and Stonewall (Stwl) (Fig. 1G). Notably, both proteins have been associated with heterochromatin repression

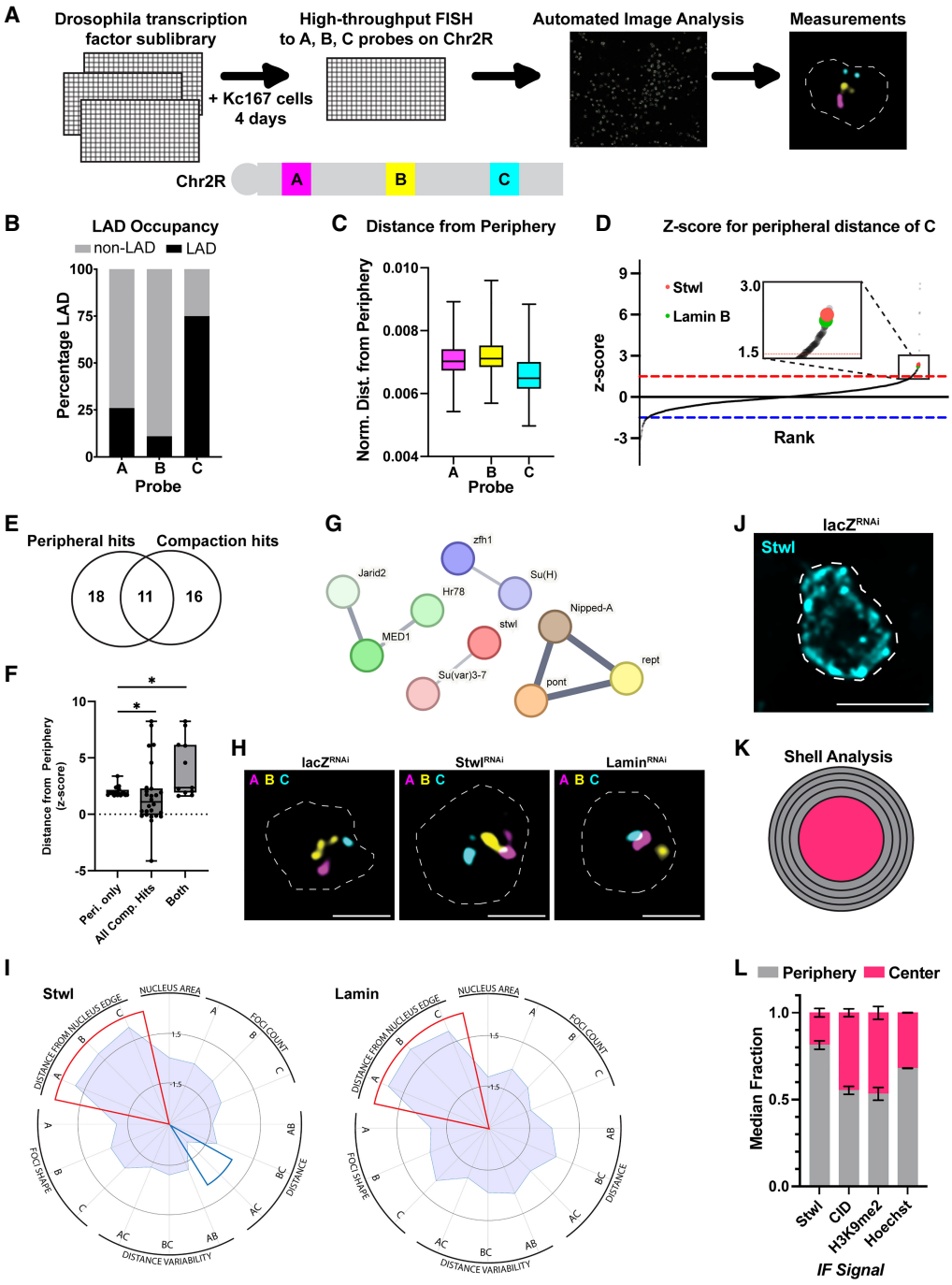

Figure 1. Discovery of novel regulators of chromatin positioning at the nuclear periphery in *Drosophila*. (*A*) Cartoon schematic of HiDRO screening pipeline and the 1 Mb probe regions along chromosome 2R. (*B*) Percentage of each chromosome 2R region occupied by LADs. (*C*) Normalized distance from periphery for each chromosome 2R region. (*D*) *Z*-score plot for genes affecting peripheral localization of chromosome 2R-C. Genes *above* the red dashed line represent hits that increase the distance between chromosome 2R-C and the nuclear periphery. These are shown larger in the overlay box. Genes *below* the blue dashed line represent hits that decrease the distance between chromosome 2R-C and the periphery. (Green) Lamin B, (red) Stwl. (*E*) Venn diagram indicating the overlap between the peripheral localization and compaction hits. Eleven genes were hits for both metrics, including *stwl*. (*F*) Comparison of *z*-scores for the normalized distance from the periphery across the categories of hits that only affect peripheral distance (Peri. only), all hits that affect compaction (All Comp. Hits), and hits that affect both peripheral distance and compaction (Both). (*G*) STRING analysis of peripheral hits. (*H*) Individual Kc167 cell nuclei labeled with probes against chromosome 2R-A (magenta), chromosome 2R-B (yellow), and chromosome 2R-C (blue) from *LacZ* RNAi (control), *stwl* RNAi, and *Lamin B* RNAi. Outlines show the nuclear boundary. (*I*) Radar plot indicating the screen metrics following Stwl knockdown (*left*) or Lamin B knockdown (*right*). Red and blue wedges represent screen metrics in which the knockdown significantly increased or decreased the metric, respectively. (*J*) Example nucleus showing Stwl immunofluorescence. Scale bar, 5 µm. (*K*) Cartoon schematic of shell analysis of immunofluorescence. The first four shells were combined to define the periphery, and the fifth shell defines the center. (*L*) Shell analysis of the indicated nuclear components. The median signal in the periphery and the center was calculated from two replicates of >300 nuclei each.

(Clark and McKearin 1996; Cléard et al. 1997; Spierer et al. 2008; Yi et al. 2009). Stwl represented one of our top hits, and, similar to *Lamin B* depletion, its phenotypic profile consisted of increased distance for all three chromosome 2R regions (Fig. 1H,I). We also note that Stwl depletion decreased chromosome arm length, as measured by the distance between chromosome 2R-A and chromosome 2R-C.

We next examined the subcellular localization of Stwl in Kc167 cells using an antibody generated against the full-length protein. Reduced immunofluorescence signal from this Stwl antibody following a 4 day dsRNA knockdown of Stwl confirmed the specificity of the antibody in Kc167 cells (Supplemental Fig. S1C–E). Consistent with published reports from other cell types, we found that Stwl was present throughout the nucleus, with an enrichment at the nuclear periphery (Fig. 1J–L; Yi et al. 2009; Rohrbaugh et al. 2013). Using a shell analysis that divided the nuclear volume into five equal-volume nested shells (Fig. 1J), we calculated the relative signal in each shell and observed that 82% of the Stwl signal occupied the nuclear periphery, while 18% occupied the center (Fig. 1K,L). In contrast, only 53% of the H3K9me2 signal and 55% of the CID/CENPA signal occupied the periphery (Fig. 1L). Total DNA as stained by Hoechst showed only 68% of signal at the periphery (Fig. 1L), suggesting that Stwl was more peripheral than expected for a random distribution throughout the nucleus. We next used affinity purification coupled with quantitative mass spectrometry to determine Stwl interactions in Kc167 cells (Supplemental Fig. S1F; Supplemental Table S2). Consistent with Stwl's perinuclear localization, we identified putative interactions with multiple components of the nuclear pore complex (NPC), including Nup214, Megator (*Drosophila* Tpr), Nup62, and Nup88. Moreover, we also identified interactions with three other "peripheral" hits from our HiDRO screen; namely, Reptin (Rept), Pontin (Pont), and CG4557. Interestingly, Rept and Pont are members of the Ino80 chromatin remodeling complex (Klymenko et al. 2006) and may be required in combination with Stwl to position or repress specific loci at the nuclear periphery. Overall, our data support a direct role for Stwl in anchoring chromatin at the nuclear periphery.

Stwl promotes perinuclear chromatin positioning independent of Lamin B in Kc167 cells

We next asked whether Stwl was required for Lamin expression or localization in Kc167 cells. qPCR and immunofluorescence quantification showed that Lamin B expression was not reduced following Stwl depletion (Supplemental Fig. S1G,H). To determine whether Stwl depletion affected the peripheral localization of Lamin B, we examined five distinct Lamin phenotypes and manually assessed >350 cells following LacZ (control) or Stwl depletion (Supplemental Fig. S1I). The overall distribution of each phenotype across four Stwl RNAi replicates was not statistically significant from LacZ depletion (Supplemental Fig. S1J), suggesting that Stwl relocalizes peripheral chromatin independent of Lamin B expression or localization.

Stwl regulates chromatin positioning at the nuclear periphery in female GSCs

stwl has been previously shown to be important for GSC self-renewal, oocyte specification, and egg chamber development in *Drosophila* ovaries (Clark and McKearin 1996; Akiyama 2002; Maines et al. 2007). Interestingly, a previous study has also shown that germ cells transform their spatial genome organization during GSC differentiation, including changes in the perinuclear positioning of chromatin (Joyce et al. 2013). However, the mechanism of Stwl function in GSC maintenance and whether it contributes to GSC genome organization remain unclear. To address this question, we turned to the *Drosophila* ovary, which is a powerful system for studying GSC fate and tissue homeostasis (Spradling et al. 2011). Each *Drosophila* ovary comprises 16–20 autonomous egg-producing units known as ovarioles. The anterior tip of each ovariole contains a germarium, which houses GSCs and differentiated germ cells (Fig. 2A). Each GSC divides asymmetrically to produce one self-renewing daughter cell (GSC) (green cell in Fig. 2A) and one differentiating daughter cell (cystoblast [CB]) (purple cell in Fig. 2A), with cystoblasts undergoing further transit-amplifying divisions to generate germline cysts (yellow cells in Fig. 2A). Crucially, the balance between GSC self-renewal and differentiation maintains tissue homeostasis; excessive self-renewal can lead to stem cell tumors, while precocious differentiation can lead to tissue atrophy.

We first depleted Stwl constitutively in early germ cells (including GSCs and CBs) by RNAi using *nos-Gal4::VP16* (Fig. 2A). As expected, we observed a severe agametic ovary phenotype upon Stwl depletion (Fig. 2B) and fully penetrant female sterility (Supplemental Fig. S2A). Moreover, these Stwl-depleted ovaries contained very few cells containing the germ cell cytoplasmic marker Vasa (Fig. 2C). Conversely, although Stwl is expressed in male germ cells, Stwl depletion using *nos-Gal4* in the male germline did not affect testis development or fertility (Supplemental Fig. S2B–D), suggesting a female germline-specific role for Stwl. Additionally, we verified the Stwl knockdown phenotype using flies carrying a precise *stwl* deletion ($stwl^{KO4}$) in *trans* to a *stwl* mutant allele ($stwl^{LL06470}$) (Supplemental Fig. S2E). Consistent with the constitutive germline knockdown of Stwl, *stwl* mutant females also exhibited substantial germ cell loss and agametic ovaries (Supplemental Fig. S2F). In contrast to the acute loss of early germ cells when Stwl was absent in GSCs, Stwl knockdown in differentiated germ cells using *bam-Gal4* did not affect germarium development (Fig. 2A,B; Supplemental Fig. S2G,H). Instead, *bam-Gal4*-mediated Stwl depletion led to downstream defects in egg chamber development (Supplemental Fig. S2I,J), with females exhibiting a strong reduction in fertility compared with controls (Supplemental Fig. S2K). The role of Stwl in later stages of oogenesis has been characterized in a separate study (Kotb et al. 2024). Altogether, these data suggest that Stwl has a critical and cell-autonomous function in female GSC maintenance.

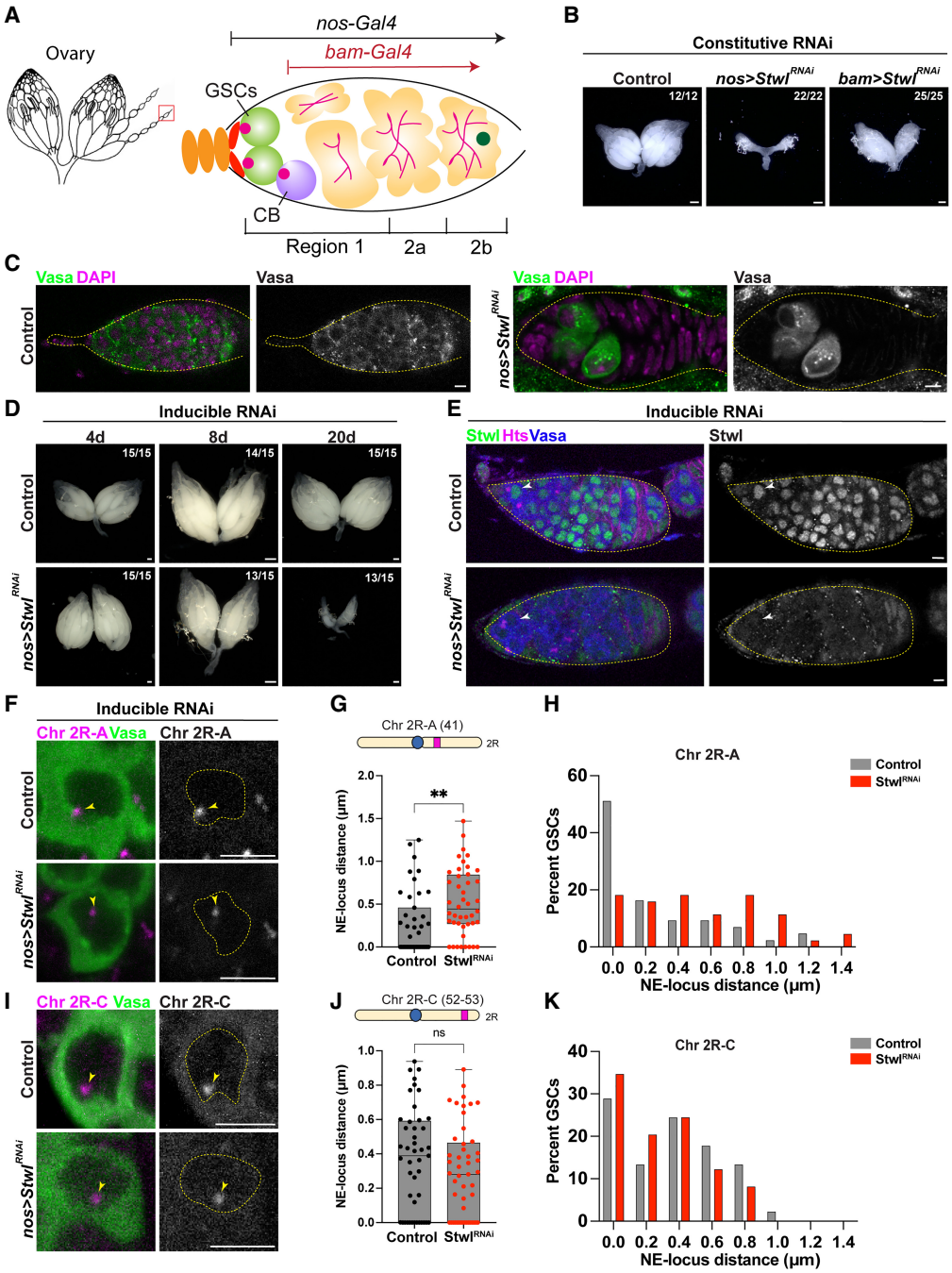

Figure 2. Stwl is a regulator of perinuclear chromatin positioning in female GSCs. (*A*) Schematic of *Drosophila* ovary and germarium. The germarium resides at the anterior tip of the ovariole (red box) and is further subdivided into region 1, containing germline stem cells (GSCs; green) and cystoblasts (CBs; purple), and regions 2a/2b, containing differentiated germ cell cysts (yellow). (*B*) Ovaries from control *TM3/Stwl*^{RNAi}, *nos>Stwl*^{RNAi}, and *bam>Stwl*^{RNAi} imaged 3 days after eclosion. Scale bars, 100 µm. (*C*) Germaria from *nos>mCherry*^{RNAi} (control) and *nos>Stwl*^{RNAi} ovaries stained for Vasa (green) and DAPI (magenta). Scale bar, 5 µm. (*D*) Ovaries from *nos>mCherry*^{RNAi} (control) and *nos>Stwl*^{RNAi} following 4, 8, and 20 day shifts to 29°C in a *Gal80*^{ts} background. Scale bars, 100 µm. (*E*) Germaria from *nos>mCherry*^{RNAi} (control) and *nos>Stwl*^{RNAi} ovaries stained for Stwl (green), Vasa (blue), and Hts (magenta) following a 4 day shift to 29°C. White arrowheads indicate the GSCs. Scale bars, 5 µm. (*F*) Oligopaint FISH against chromosome 2R-A (magenta) and IF staining of Vasa (green) in GSCs from *nos>mCherry*^{RNAi} (control) and *nos>Stwl*^{RNAi} ovaries following a 4 day shift to 29°C. Yellow arrowheads indicate the chromosome 2R-A locus within the nucleus. Yellow dotted lines indicate the nuclear boundary. Scale bars, 5 µm. (*G*) Quantification of the NE–chromosome 2R-A distance (in micrometers) in GSCs from *F*. $n = 43$ GSCs from *nos>mCherry*^{RNAi}; $n = 44$ GSCs from *nos>Stwl*^{RNAi}. (**) $P < 0.01$ from Student's *t*-test. (*H*) Histogram of the NE–chromosome 2R-A distance (in micrometers) in GSCs from *G*. (*I*) Oligopaint FISH against chromosome 2R-C (magenta) and IF staining of Vasa (green) in GSCs from *nos>mCherry*^{RNAi} (control) and *nos>Stwl*^{RNAi} ovaries following a 4 day shift to 29°C. Yellow arrowheads indicate the chromosome 2R-C locus within the nucleus. Yellow dotted lines indicate the nuclear boundary. Scale bars, 5 µm. (*J*) Quantification of the NE–chromosome 2R-C distance (in micrometers) in GSCs from *I*. $n = 45$ GSCs from *nos>mCherry*^{RNAi} (control); $n = 49$ GSCs from *nos>Stwl*^{RNAi}. (ns) $P > 0.05$ from Student's *t*-test. (*K*) Histogram of the NE–chromosome 2R-C distance (in micrometers) in GSCs from *J*.

To elucidate the series of events linking Stwl depletion to GSC loss, we used an inducible knockdown system comprising a temperature-sensitive allele of Gal80 (*Gal80^{ts}*) and *nos-Gal4*. Here, germ cell-specific Gal4 expression is only induced upon shifting the adult flies to 29°C (due to inactivation of *Gal80^{ts}*), triggering RNAi and subsequent protein depletion. Using this system, we recapitulated the agametic ovary phenotype observed upon constitutive Stwl depletion 20 days after shift to 29°C (Fig. 2D). Importantly, we observed that Stwl was depleted in early female germ cells starting from 4 days after shift to 29°C (Fig. 2E). Therefore, all further Stwl depletion experiments were performed in flies shifted for 4–6 days to 29°C.

Based on our screen and our phenotypic data in Kc167 cells, we hypothesized that Stwl might position chromatin at the nuclear periphery in female GSCs. Therefore, we first assessed the position of the chromosome 2R regions (A and C) in female GSCs using Oligopaint DNA FISH. Specifically, we measured the shortest distance of these loci from the GSC nuclear boundary, which was marked by the NE-proximal cytoplasmic protein Vasa. We observed that chromosome 2R-A was positioned closest to the nuclear periphery in control GSCs (median distance = 0 µm) (Fig. 2F–H). In the absence of Stwl, however, this locus was primarily observed in the nuclear interior (median distance = 0.44 µm) (Fig. 2F–H). In contrast to region A, chromosome 2R-C did not exhibit peripheral localization in control GSCs (median distance = 0.39 µm), consistent with cell type-specific LAD composition, and, as such, its position remained unaffected following Stwl depletion (median distance = 0.28 µm) (Fig. 2I–K). We further examined the position of centromeres (marked by the centromeric histone Cid/dCENP-A) in GSC nuclei, as they are often observed in proximity to the NE in many cell types (Chaly and Munro 1996; Mayer et al. 2005; Hou et al. 2012). While control GSCs exhibited a substantial number of NE-proximal centromeres (Supplemental Fig. S3A–C), centromeres in Stwl-depleted GSCs were relocalized to the nuclear interior (Supplemental Fig. S3A–C). Consistent with our data from Kc167 cells, Stwl positions chromatin at the nuclear periphery in female GSCs.

Reduced peripheral chromatin localization in the absence of Stwl is associated with gaps in the nuclear lamina

We next asked whether Stwl localized to the nuclear periphery in female GSCs as observed in Kc167 cells. We used ovaries from newly eclosed females as well as ovaries enriched for GSC-like cells using *bag-of-marbles* (*bam*) mutants (McKearin and Ohlstein 1995) and stained for Stwl following methanol fixation, a method that can expose otherwise inaccessible epitopes. Interestingly, we observed that a fraction of Stwl consistently localized at the nuclear periphery and was closely associated with the nuclear lamina and the nuclear pore complexes (NPCs) (Fig. 3A; Supplemental Fig. S4A,B), which agrees with our observations in cultured cells. We next sought to identify the underlying cause of the changes in the peripheral chromatin localization observed in Stwl-depleted GSCs. As loss of nuclear envelope integrity is associated with reduced perinuclear chromatin (Shevelyov et al. 2009; Kohwi et al. 2013; Chen et al. 2014), we assessed whether Stwl depletion affected NE components in GSCs. We first checked the localization of Lamin B (lamin Dm0) and Lamin C in the Stwl-depleted GSCs, since these proteins at the inner nuclear membrane (INM) are associated with peripheral chromatin. We observed that 38% of Stwl-depleted GSCs exhibited stretches of the NE lacking nuclear lamins (referred to here as lamina gaps), with these gaps spanning 10%–40% of the nuclear envelope (Fig. 3B,C; Supplemental Fig. S4C–F). Importantly, the gaps appeared to be specific to lamins, since other INM proteins such as Otefin (*Drosophila* Emerin ortholog) (Supplemental Fig. S4G,H) and the Lamin B receptor (LBR) (Supplemental Fig. S4I,J) were still present at the gaps. Moreover, we noticed an increased signal intensity of nuclear pore complexes (NPCs) in certain regions of the lamina gaps (Fig. 3B,C; Supplemental Fig. S4K–N), consistent with previous reports indicating that NPCs can cluster in regions lacking the nuclear lamina (Xie et al. 2016; Cheng et al. 2021).

To further assess the underlying chromatin ultrastructure at the nuclear periphery, we performed transmission electron microscopy (TEM) in control and Stwl-depleted GSC-enriched ovaries. In contrast to the NE from terminally differentiated mammalian cells, which are lined with compact and electron-dense heterochromatin (van Steensel and Belmont 2017), *Drosophila* GSCs exhibited multiple distinct perinuclear electron-dense chromatin foci, likely reflecting peripherally localized heterochromatin. In the control, we observed approximately one electron-dense chromatin focus associated with the nuclear periphery per micrometer of the nuclear envelope (Fig. 3D,F). In contrast, Stwl-depleted GSC nuclei exhibited an approximately twofold reduction in the perinuclear electron-dense chromatin foci (Fig. 3E,F). In addition, we observed tracts of clustered NPCs in Stwl-depleted GSCs (Fig. 3E, arrowheads mark the position of the NPC cluster), which likely correspond to the lamina gaps observed by immunofluorescence staining (Fig. 3B,C; Supplemental Fig. S4K). We next asked whether Stwl depletion led to loss of NPCs from the NE or whether they were instead reorganized across the nucleus. We observed that the normalized number of NPCs (NPCs per micrometer of the NE) remained unchanged across both control and Stwl-depleted GSCs, suggesting that NPCs are reorganized into clusters in the absence of Stwl (Fig. 3G). Notably, almost no electron-dense chromatin foci were found in NE stretches with NPC clusters, which correspond to lamina gaps (Fig. 3H). Consistently, Stwl-depleted GSCs with lamina gaps exhibited fewer NE-proximal centromeric foci in comparison with control GSCs and Stwl-depleted GSCs with an intact lamina (Supplemental Fig. S3A–C). Taken together, our data suggest that gaps in the nuclear lamina likely contribute to impaired chromatin localization at the nuclear periphery in Stwl-depleted GSCs.

Despite not observing a role for Stwl in Lamin B expression in cultured cells (Supplemental Fig. S1G,H), we

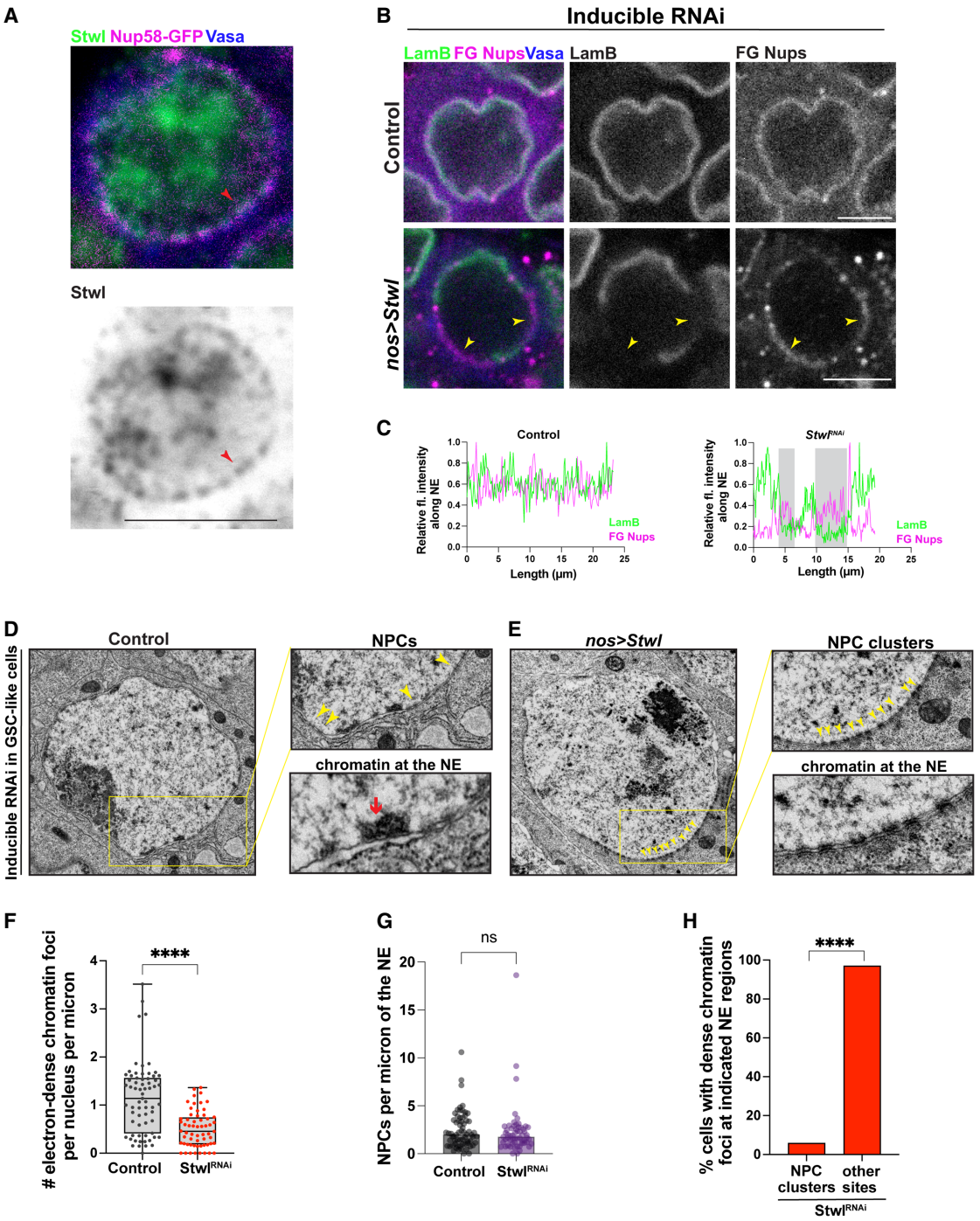

Figure 3. Loss of Stwl leads to defects in perinuclear chromatin organization. (*A*) IF staining of Stwl (green) and Vasa (blue) in GSCs from young ovaries in a *Nup58-GFP* (magenta) strain. Scale bar, 5 µm. (*B*) IF staining of Lamin B (green), FG Nups (magenta), and Vasa (blue) in GSCs from *nos>mCherry*^{RNAi} (control) and *nos>Stwl*^{RNAi} ovaries following a 4 day shift to 29°C. Yellow arrowheads indicate NPC clusters in the regions lacking Lamin B. Scale bars, 5 µm. (*C*) Relative fluorescence intensity of Lamin B (green) and FG Nups (magenta) along the nuclear envelope from *B*. Shaded gray regions highlight NPC clustering in regions lacking Lamin B. (*D*) TEM image of GSC-like cells from *nos>mCherry*^{RNAi} (control) ovaries in a *bam*$^{\Delta 86}$/*bam*^{1} background following a 4 day shift to 29°C. The *top inset* shows NPCs (yellow arrowheads), while the *bottom inset* shows an electron-dense chromatin focus associated with the nuclear envelope. (*E*) TEM image of GSC-like cells from *nos>Stwl*^{RNAi} ovaries in a *bam*$^{\Delta 86}$/*bam*^{1} background following a 4 day shift to 29°C. The *top inset* shows NPC clusters, while the *bottom inset* shows the absence of electron-dense chromatin foci in regions containing NPC clusters. (*F*) Quantification of perinuclear electron-dense chromatin foci in GSC-like cells from *D* and *E*. Each dot represents the number of perinuclear chromatin foci per nucleus per micrometer of the nuclear envelope. $n = 67$ GSCs from *nos>mCherry*^{RNAi}; $n = 60$ GSCs from *nos>Stwl*^{RNAi}. (****) $P < 0.0001$ from Student's *t*-test. (*G*) The number of NPCs per micrometer of the NE was quantified from TEM images of GSC-like cells from *nos>mCherry*^{RNAi} (control; $n = 66$) and *nos>Stwl*^{RNAi} ($n = 59$) ovaries in a *bam*$^{\Delta 86}$/*bam*^{1} background following a 4 day shift to 29°C. (ns) $P > 0.05$ from Student's *t*-test. (*H*) The percentage of perinuclear electron-dense chromatin foci at NPC clusters versus other regions on the nuclear envelope in GSC-like cells from *E*. $n = 42$. (****) $P < 0.0001$ from Fisher's exact test.

considered that reduced levels of Lamin B in Stwl-depleted GSCs could be a possible cause of the lamina gaps and lead to GSC loss. To test this, we used Gal4-mediated *Lamin B* overexpression in the female germline. Lamin B overexpression is known to result in cytoplasmic lamin accumulations in *Drosophila* intestinal stem cells (ISCs) and enterocytes (ECs) (Petrovsky et al. 2018). Consistently, we observed similar cytoplasmic lamin accumulations following *Lamin B* overexpression in GSCs (Supplemental Fig. S5A,B). However, Lamin B overexpression in Stwl mutant GSCs failed to rescue the lamina gaps or the atrophied ovary phenotype (Supplemental Fig. S5C,D,F). These data suggest that a decrease in Lamin B protein levels is not a primary cause of lamina gaps and GSC loss in the absence of Stwl. Given the known roles of the nuclear lamina and NPCs in tethering chromatin at the nuclear periphery (Pickersgill et al. 2006; Gozalo et al. 2020; Iglesias et al. 2020), we also tested whether heterozygous mutations of *Lamin B* or a Stwl-interacting nucleoporin (*Nup214*) (Supplemental Fig. S1F) affected germ cell loss in the absence of Stwl. Interestingly, we found that a reduced dose of *Lamin B* (but not *Nup214*) enhanced germ cell loss in *stwl* mutant ovaries (Supplemental Fig. S5E, F), suggesting that Lamin B and Stwl may possess complementary roles in GSC maintenance.

Recent reports have shown that loss of the INM protein Otefin triggers a *Chk2*-dependent GSC developmental arrest in *Drosophila* ovaries, with *Chk2* mutation completely restoring oogenesis in the absence of Otefin (Barton et al. 2013). However, *Chk2* and *stwl* double mutants did not rescue GSC loss or ovary atrophy (Supplemental Fig. S5G). Finally, we tested whether germ cell death markers such as lysotracker and death caspase 1 (Dcp-1) were elevated in Stwl-depleted germaria (Yacobi-Sharon et al. 2013). While we did observe cell death in the absence of Stwl, the death was restricted to differentiated germline cysts and not observed in GSCs (Supplemental Fig. S5H,I). Thus, our data point to a distinct mechanism for GSC loss and ovary atrophy in the absence of Stwl.

Stwl represses the expression of the GSC differentiation gene benign gonial cell neoplasm *(*bgcn*)*

Based on our FISH and TEM data, we hypothesized that loss of peripheral chromatin organization in the absence of Stwl might contribute to GSC loss through altered transcriptional programs. To test this, we first wanted to identify the Stwl-dependent transcriptome, specifically in GSC-like cells. Although other studies have identified Stwl-dependent gene expression in ovaries, these studies were performed in young ovaries that contain early egg chambers, differentiated germline cysts, and GSCs (Zinshteyn and Barbash 2022; Kotb et al. 2024). Moreover, Stwl-depleted ovaries rapidly lose GSCs (Fig. 2B,C) and are therefore unsuitable for RNA-seq experiments that seek to determine the GSC transcriptome. However, a previous study has shown that overexpression of Stwl in GSCs leads to a subtle increase in the number of undifferentiated germ cells in the ovary (Maines et al. 2007). Interestingly, we found that Stwl overexpression further enhanced the number of undifferentiated (Bam-negative) germ cells in a *bam* heterozygous background, where GSC differentiation signaling is likely weakened (Fig. 4A,B). These data further strengthen the idea that Stwl overexpression can promote GSC fate. We therefore performed RNA-seq to identify Stwl-dependent genes in control and Stwl-overexpressing ($Stwl^{OE}$) GSC-enriched ovaries. We observed 548 genes differentially expressed following Stwl overexpression ($\log_2FC > |0.6|$, $P_{adj} < 0.01$), with 154 genes downregulated in comparison with the control (Fig. 4C; Supplemental Tables S3, S4). We specifically focused on the downregulated genes, since Stwl is reported to function as a transcriptional repressor (Clark and McKearin 1996; Maines et al. 2007; Yi et al. 2009). Here, we found that expression of the GSC differentiation gene *benign gonial cell neoplasm* (*bgcn*) (Lavoie et al. 1999; Ohlstein et al. 2000; Li et al. 2009), the loss of which results in the accumulation of undifferentiated GSC-like cells in the *Drosophila* ovary, was reduced 1.9-fold upon Stwl overexpression (Fig. 4C,D). In addition, we identified that an inhibitor of ecdysone signaling, the transcriptional corepressor *SMRT-related and ecdysone receptor-interacting factor* (*Smr*) (Heck et al. 2012), was also downregulated 1.5-fold following Stwl overexpression (Fig. 4C,D). Since ecdysone signaling is critical for GSC self-renewal and maintenance (Ables and Drummond-Barbosa 2010), Smr activity may promote differentiation and is likely repressed in GSCs. Interestingly, both *bgcn* and *Smr* are upregulated in gene expression data sets from other studies using Stwl-depleted ovaries (Maines et al. 2007; Zinshteyn and Barbash 2022; Kotb et al. 2024), suggesting that these genes are likely repressed in a Stwl-dependent manner (Fig. 4C). Furthermore, we performed cleavage under targets and release using nuclease (CUT&RUN) (Meers et al. 2019) chromatin profiling experiments in GSC-enriched ovaries to identify the direct targets of Stwl (Fig. 4E). We observed Stwl peaks mostly at noncoding sequences such as promoters (~47%) but also at introns, UTRs, and distal intergenic regions (Fig. 4E; Supplemental Fig. S6A). Moreover, we found that Stwl-bound sequences were enriched for motifs associated with context-specific reduction of gene expression (Supplemental Fig. S6B; Yang et al. 2002; Vallone et al. 2004; Li and Gilmour 2013). We next assessed the extent of overlap between Stwl-bound loci in GSCs and differentially expressed genes upon Stwl overexpression. We found that 59.1% of downregulated genes and 69.5% of upregulated genes had a Stwl peak within 1 kb of the gene body (Supplemental Fig. S6C). By combining our RNA-seq and CUT&RUN data, we identified 15 genes that were bound by Stwl in GSCs, downregulated following Stwl overexpression, and shown to be upregulated in young ovaries lacking Stwl (Supplemental Table S3; Zinshteyn and Barbash 2022; Kotb et al. 2024). These genes included both *bgcn* and *Smr* (Fig. 4F; Supplemental Fig. S6D), further indicating that Stwl may directly bind and regulate the expression of these genes.

Stwl positions bgcn *at the nuclear periphery to regulate its expression*

Our data thus far indicate that Stwl can position chromatin at the nuclear periphery in GSCs and repress bona fide

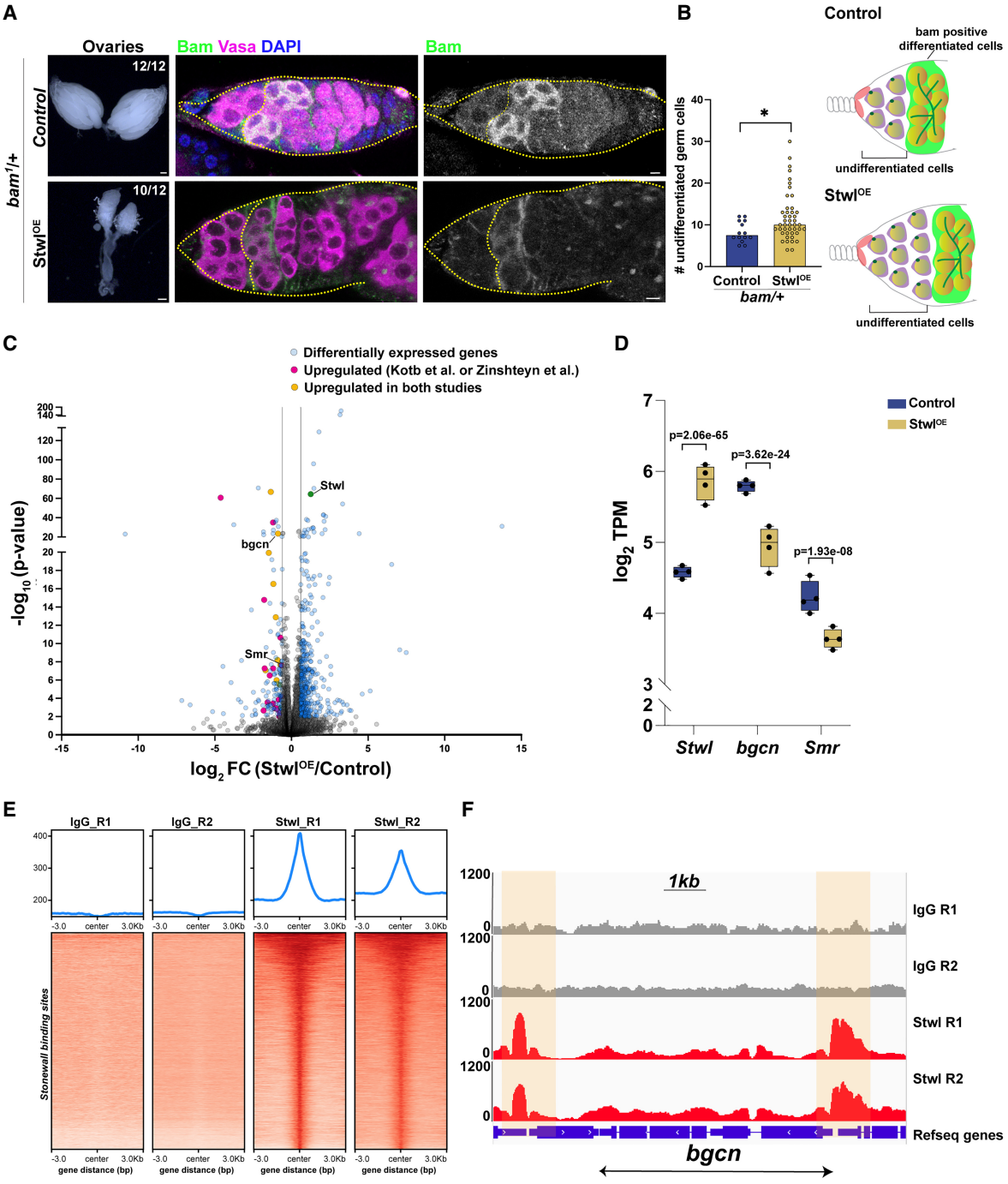

Figure 4. Stwl binds and represses the *bgcn* differentiation gene. (*A*, *left* panels) *nos; TM3* (control) and *nos>Stwl*^{EY00146} (*Stwl*^{OE}) ovaries in a *bam*^{1}/+ background. (*Middle* and *right* panels) IF staining of Bam (green), Vasa (magenta), and DAPI (blue) in germaria. Scale bars, 5 µm. (*B*) Quantification of undifferentiated Bam-negative germ cells from *A*. $n = 15$ germaria from the control; $n = 45$ germaria from *stwl*^{OE}. (*) $P < 0.05$ from a Student's *t*-test. (*C*) Volcano plot of $-\log_{10}$(*P*-value) versus $\log_2$FC from *nos-Gal4*/+ (control) and *nos>stwl*^{EY00146} (*Stwl*^{OE}) GSC-enriched ovaries (*bam*$^{\Delta 86}$/*bam*^{1} background). Differentially expressed genes ($\log_2$FC > |0.6|, $P_{adj} < 0.01$) are indicated as blue dots. Genes upregulated in Stwl-depleted ovaries from Zinshteyn and Barbash (2022) or Kotb et al. (2024) are indicated as magenta dots, while genes upregulated in both studies are indicated as yellow dots. Adjusted *P*-values following multiple testing correction are shown. (*D*) Transcripts per million ($\log_2$TPM) for the indicated genes from *nos-Gal4*/+ (control) and *nos>stwl*^{EY00146} (*Stwl*^{OE}) GSC-enriched ovaries in a *bam*$^{\Delta 86}$/*bam*^{1} background. Adjusted *P*-values following multiple testing correction are shown. (*E*) Heat maps of CUT&RUN reads for IgG from young WT ovaries and for Stwl from ovaries enriched for GSC-like cells (*nos>bam*^{RNAi}). Data are centered on ±3 kb window around 12,888 Stwl peaks (merged within 1 kb) and are shown for two replicates each. (*F*) Capture of the IGV genome browser (v2.11.4) showing an ~10 kb region on *Drosophila* chromosome 3 (*y*-axis indicates reads per kilobase per million reads). (Blue) Ensembl genes. Shaded areas correspond to Stwl binding peaks.

GSC differentiation genes such as *bgcn*. To test whether these two functions of Stwl were linked, we first assessed the position of the *bgcn* locus in relation to the GSC nuclear periphery using Oligopaint DNA FISH. We measured the shortest distance between the *bgcn* locus and the nuclear periphery in control and Stwl-depleted GSCs. We observed a twofold reduction in *bgcn* loci at the nuclear periphery of GSCs in the absence of Stwl (control GSCs: 37.3% peripheral *bgcn* loci; Stwl-depleted GSCs: 19% peripheral *bgcn* loci) (Fig. 5A–C). We also assessed the position of the *bgcn* locus in cystoblasts and differentiated germline cysts within the germarium (region 2a/2b) (Fig. 2A). Similar to GSCs, we observed a 1.6-fold reduction in peripherally localized *bgcn* loci in Stwl-depleted CBs (control CBs: 47% peripheral *bgcn* loci; Stwl-depleted CBs: 28% peripheral *bgcn* loci) (Supplemental Fig. S7A,B) and a 1.5-fold reduction in peripherally localized *bgcn* loci in Stwl-depleted germline cysts (control cysts: 61% peripheral *bgcn* loci; Stwl-depleted cysts: 39% peripheral bgcn loci) (Fig. 5D–F). The increased peripheral localization of *bgcn* loci in differentiated germline cysts in comparison with GSCs (61% in germline cysts vs. 37.3% in GSCs) is consistent with the observation that *bgcn* expression is typically only observed in GSCs and CBs (Ohlstein et al. 2000). We next assessed whether *Smr* was positioned at the nuclear periphery in GSCs and whether this perinuclear positioning was Stwl-dependent. We found that 50.5% of *Smr* loci were positioned at the nuclear periphery in control GSCs and observed a twofold reduction in *Smr* perinuclear positioning upon Stwl depletion (Supplemental Fig. S7C–E). Although 37.2% of *Smr* loci were positioned at the nuclear periphery in CBs, this perinuclear positioning was unaffected in the absence of Stwl (Supplemental Fig. S7F,G). Finally, we tested whether the nuclear position of a housekeeping gene (*Gapdh1*) or a germline-expressed gene not bound by Stwl (*Ord*) was altered in Stwl-depleted GSCs and CBs. Unlike *bgcn* and *Smr*, both *Gapdh1* and *Ord* were primarily localized in the nuclear interior in GSCs and CBs, and their position relative to the nuclear periphery was unchanged in the absence of Stwl (Supplemental Fig. S7H–P). Similarly, the interlocus distance between *Ord* and *Gapdh1*, both of which are on chromosome 2R, was also independent of Stwl (Supplemental Fig. S7Q).

Interestingly, we observed that both the *bgcn* and *Smr* gene loci were occasionally unpaired in GSCs (Supplemental Fig. S7R,S), potentially giving rise to a situation in which one allele could be positioned in the nuclear interior and expressed even while the other allele is silenced at the nuclear periphery. Therefore, we simultaneously assessed the position of all *bgcn* and *Smr* loci to determine the percentage of GSCs where these genes were positioned at the nuclear periphery and presumably inactive. We observed that 63% of control GSCs contained at least one of the genes at the nuclear periphery irrespective of the pairing status (Fig. 5G,H). In contrast, only 28.4% of Stwl-depleted GSCs contained perinuclear *bgcn* and/or *Smr* (Fig. 5G,H). Strikingly, there was a ninefold reduction in GSCs containing both *bgcn* and *Smr* at the nuclear periphery in Stwl-depleted GSCs (Fig. 5H). Together, our data indicate that Stwl promotes perinuclear positioning of target loci such as *bgcn* and *Smr* in GSCs. In the absence of Stwl, multiple such target loci may simultaneously relocalize to the nuclear interior, where they could be precociously expressed and tilt the delicate balance between GSC self-renewal and differentiation, thus affecting stem cell maintenance.

Does the position of a Stwl-bound gene locus within the nucleus dictate its expression? To address this question, we performed single-molecule RNA FISH (smFISH) targeting *bgcn* transcripts in control and Stwl-depleted ovaries. We used FISH probes targeting *bgcn* exons, which mark cytoplasmic *bgcn* mRNA molecules as well as nascent transcripts emanating from the *bgcn* gene locus. In control cells, cytoplasmic *bgcn* transcripts were primarily observed in the GSCs and cystoblasts (Fig. 5I), consistent with previous reports (Ohlstein et al. 2000) and correlating with the increased protein expression of Stwl from GSCs to the germ cell cysts in region 2a/2b (Supplemental Fig. S8A). In contrast, Stwl depletion resulted in cytoplasmic *bgcn* transcripts across the entire germarium, including differentiated germline cysts in region 2a/2b (Fig. 5J; Supplemental Fig. S8B). Importantly, we observed significantly more CBs and differentiated germline cysts with nascent *bgcn* transcription upon Stwl depletion (Fig. 5K), which strongly correlates with a reduced frequency of *bgcn* loci at the nuclear periphery (Fig. 5A–F; Supplemental Fig. S7A,B).

Strikingly, nearly all *bgcn* nascent transcription in control and Stwl-depleted GSCs was observed in the nuclear interior (Fig. 5L). For example, although 37.3% of *bgcn* gene loci are perinuclear in control GSCs, *bgcn* nascent transcription was predominantly observed in the nuclear interior (92% of control GSCs with *bgcn* nascent transcription) (Fig. 5M). This suggests that the majority of perinuclear *bgcn* gene loci are transcriptionally silent. We observed a similar effect in Stwl-depleted GSCs, where *bgcn* nascent transcription was again primarily observed in the nuclear interior (89% of Stwl-depleted GSCs with *bgcn* nascent transcription) (Fig. 5N). Thus, the *bgcn* loci that remain at the nuclear periphery are not transcribed, even in Stwl-depleted GSCs. These data suggest that the primary function of Stwl may be to position specific chromatin loci or genes at the nuclear periphery, where they are kept transcriptionally silent through the action of other factors. Taken together, we propose a model in which Stwl promotes GSC fate through perinuclear positioning and repression of differentiation genes such as *bgcn*.

Discussion

The regulation of gene expression is a primary mechanism that dictates cell fate. In addition to local factors influencing gene expression such as enhancer–promoter contacts and sequence-specific transcription factors, the position of a gene within the nucleus can also influence expression (Meister and Taddei 2013; van Steensel and Belmont 2017; Guerreiro and Kind 2019). In many organisms, the enrichment of dense and compact heterochromatin at the

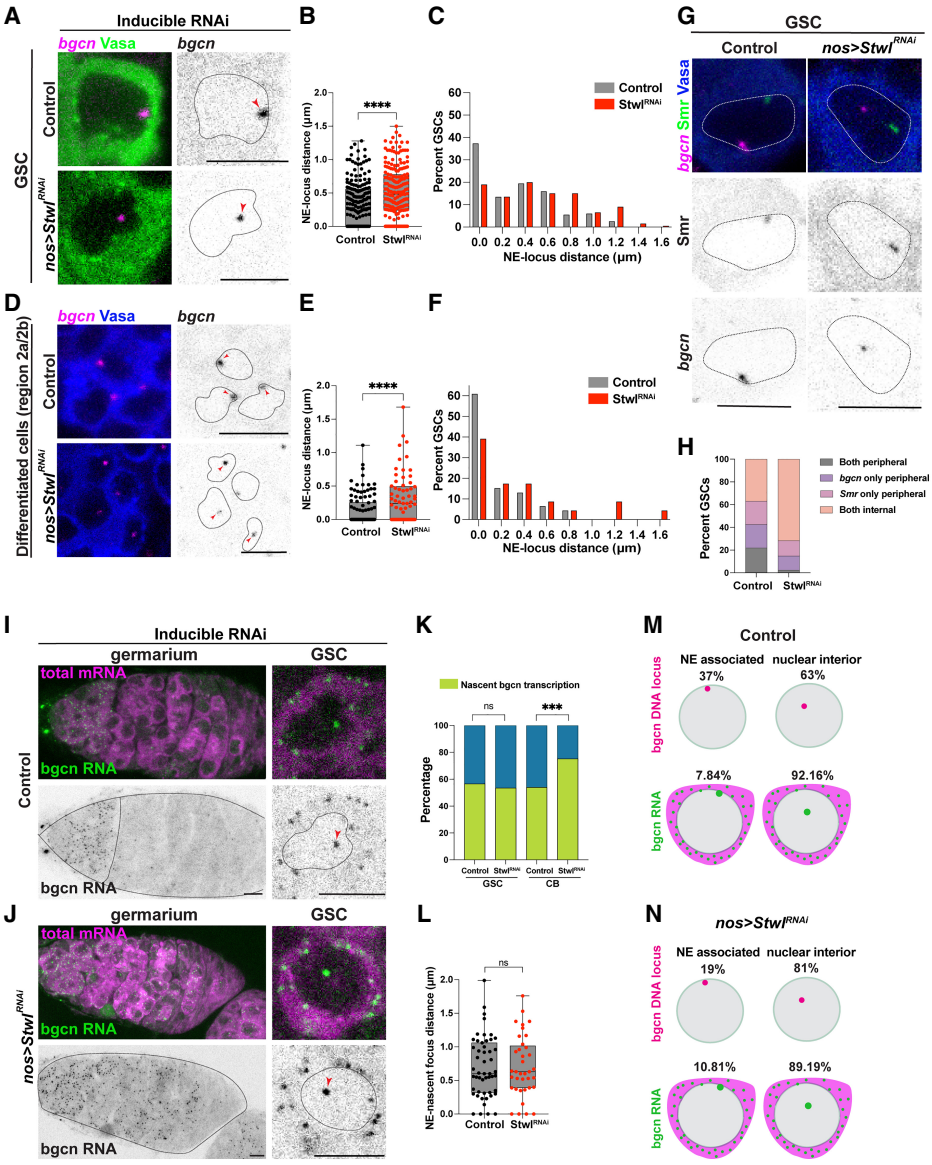

Figure 5. Stwl positions *bgcn* at the nuclear periphery in female GSCs. (*A*) Oligopaint FISH against the *bgcn* locus (magenta) and IF staining of Vasa (green) in GSCs from *nos>mCherry*^{RNAi} (control) and *nos>Stwl*^{RNAi} ovaries following a 6 day shift to 29°C. Red arrowheads indicate the *bgcn* locus within the nucleus. Black dotted lines indicate the nuclear boundary. Scale bars, 5 µm. (*B*) Quantification of the NE–*bgcn* distance (in micrometers) in GSCs from *A*. $n = 201$ GSCs from *nos>mCherry*^{RNAi} (control); $n = 200$ GSCs from *nos>Stwl*^{RNAi}. (****) $P < 0.0001$ from Student's *t*-test. (*C*) Histogram of the NE–*bgcn* distance (in micrometers) in GSCs from *B*. (*D*) Oligopaint FISH against the *bgcn* locus (magenta) and IF staining of Vasa (blue) in region 2a/2b differentiated germline cysts from *nos>mCherry*^{RNAi} (control) and *nos>Stwl*^{RNAi} ovaries following a 6 day shift to 29°C. Black dotted lines indicate the nuclear boundary. Scale bars, 5 µm. (*E*) Quantification of the NE–*bgcn* distance (in micrometers) in region 2a/2b differentiated germ cells from *D*. $n = 106$ GSCs from *nos>mCherry*^{RNAi} (control); $n = 65$ GSCs from *nos>Stwl*^{RNAi}. (****) $P < 0.0001$ from Student's *t*-test. (*F*) Histogram of the NE–*bgcn* distance (in micrometers) in region 2a/2b differentiated germ cells from *E*. (*G*) Oligopaint FISH against the *bgcn* locus (magenta) and *Smr* locus (green) and IF staining of Vasa (blue) in GSCs from *nos>mCherry*^{RNAi} (control) and *nos>Stwl*^{RNAi} ovaries following a 6 day shift to 29°C. Red arrowheads indicate the *bgcn* locus within the nucleus. Black dotted lines indicate the nuclear boundary. Scale bars, 5 µm. (*H*) Quantification of the percentage of GSCs with the indicated categories that relate to the peripheral and internal positions of *bgcn* and *Smr* loci. $n = 35$ GSCs from *nos>mCherry*^{RNAi} (control); $n = 54$ GSCs from *nos>Stwl*^{RNAi}. (*I*) smFISH against *bgcn* mRNA (green) and poly-A mRNA (magenta) in GSCs from *nos>mCherry*^{RNAi} (control) following a 6 day shift to 29°C. In the *bottom left* panel, black dotted lines demarcate region 1 and the germarium boundary. In the *bottom right* panel, black dotted lines indicate the nuclear boundary. Scale bars, 5 µm. (*J*) smFISH against *bgcn* mRNA (green) and poly-A mRNA (magenta) in GSCs from *nos>Stwl*^{RNAi} following a 6 day shift to 29°C. In the *bottom left* panel, black dotted lines demarcate the germarium boundary. In the *bottom right* panel, black dotted lines indicate the nuclear boundary. Scale bars, 5 µm. (*K*) Quantification of the percentage of GSCs and cystoblasts (CBs) with nascent bgcn expression from *nos>mCherry*^{RNAi} (control) and *nos>Stwl*^{RNAi} ovaries following a 6 day shift to 29°C. For the control, $n = 90$ GSCs and $n = 174$ CBs. For *nos>Stwl*^{RNAi}, $n = 71$ GSCs and $n = 146$ CBs. (ns) $P > 0.05$, (***) $P < 0.001$ from a Fisher's exact test. (*L*) Quantification of the NE–*bgcn* nascent focus distance (in micrometers) in GSCs from *I* and *J*. $n = 51$ GSCs from *nos>mCherry*^{RNAi} (control); $n = 37$ GSCs from *nos>Stwl*^{RNAi}. (ns) $P > 0.05$ from Student's *t*-test. (*M*,*N*) Schematic of data from *A*–*C* and *I*–*L* showing the percentage of GSCs with the *bgcn* DNA locus and the nascent *bgcn* RNA focus positioned at the nuclear periphery or in the nuclear interior in GSCs from *nos>mCherry*^{RNAi} (control) and *nos>Stwl*^{RNAi} ovaries following a 6 day shift to 29°C.

nuclear periphery gives rise to a gene-repressive nuclear subcompartment. Consistently, genes anchored to the nuclear periphery are generally transcriptionally inactive, while repositioning the same genes to the nuclear interior is associated with their expression (van Steensel and Belmont 2017; Guerreiro and Kind 2019). In many species, INM-associated proteins and repressive chromatin modifications mediate large-scale chromatin tethering to the nuclear envelope (Ungricht and Kutay 2017; van Steensel and Belmont 2017; Guerreiro and Kind 2019). However, chromatin-associated proteins that position specific gene loci at the nuclear periphery are largely unidentified, even in powerful multicellular model organisms such as *Drosophila*.

In this study, we deployed HiDRO (Park et al. 2023) in tandem with a high-throughput RNAi screen for factors influencing nuclear architecture in *Drosophila*. We identified 29 hits affecting chromatin positioning at the nuclear periphery, including multiple heterochromatin-associated proteins such as Su(var)3-7, HP2, and Jarid2, as well as transcription factors such as Su(H), Sry-δ, and Fer2, with many of these hits known to have important roles in specific cell types (Morel and Schweisguth 2000; Shaffer et al. 2002; Spierer et al. 2008; Herz et al. 2012; Tas et al. 2018). Among these hits, we have revealed that Stonewall (Stwl), a MADF-BESS transcriptional regulator previously implicated in female GSC maintenance (Clark and McKearin 1996; Akiyama 2002; Maines et al. 2007), is a novel factor positioning chromatin at the nuclear periphery in *Drosophila* cultured cells and female GSCs (Fig. 6). Using a multimodal approach, we identified that Stwl binds and represses many genes in female GSCs, including canonical differentiation genes such as *bgcn* as well as genes implicated in differentiation such as *Smr*. We propose that Stwl-mediated repression of multiple such genes through perinuclear positioning preserves the balance between self-renewal and differentiation, thereby ensuring the long-term maintenance of the GSC reservoir and preserving tissue homeostasis (Fig. 6).

Although the nuclear periphery is considered to be a repressive nuclear subcompartment (van Steensel and Belmont 2017), whether perinuclear gene position dictates transcriptional activity or whether transcriptional activity drives perinuclear positioning of genes has remained incompletely understood. Our identification of novel perinuclear anchors such as Stwl and the genomic loci that they bind and repress highlights a path forward to address this challenging question. For example, Oligopaint DNA FISH experiments revealed that the Stwl-bound *bgcn* gene locus was often positioned at the nuclear periphery in GSCs and differentiated germline cysts. This perinuclear positioning was reduced 1.5-fold to twofold in the absence of Stwl and was broadly associated with increased *bgcn* expression across the germaria as detected by smFISH. Interestingly, *bgcn* nascent transcription was primarily observed in the nuclear interior and rarely observed at the nuclear periphery in the same cell types. We observed a similar lack of *bgcn* nascent transcription at the nuclear periphery in GSCs lacking Stwl. Since the *bgcn* locus is present at the nuclear periphery in 37.3% and 19% of control and Stwl-depleted GSCs, respectively, our data are consistent with a model in which Stwl primarily functions to position loci at the nuclear periphery and in which other components of the perinuclear heterochromatin subcompartment mediate direct transcriptional repression. However, Stwl may also have other complementary roles that facilitate transcriptional repression at bound loci. For example, Stwl may possess a direct transcriptional repression activity that only operates at the nuclear periphery, potentially through interactions with specific NE-associated proteins.

Cytologically, we observed that a fraction of Stwl localizes to the nuclear periphery in both cultured *Drosophila* cells and female GSCs. Moreover, we identified interactions between Stwl and NPC proteins (Nup62, Nup88, Nup214, and Tpr/Megator) through quantitative proteomics in cultured cells. While it is possible that these interactions could facilitate nuclear import of Stwl, recent

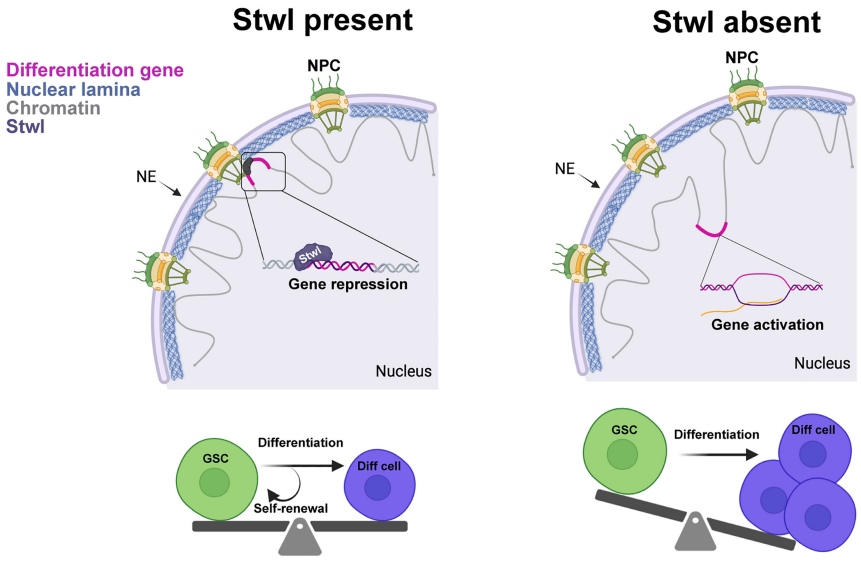

Figure 6. Model of Stwl function in female germline stem cells. Stwl-mediated positioning and repression of differentiation genes at the nuclear periphery promote the maintenance of germline stem cell fate.

studies have also shown that the perinuclear localization of active and repressive chromatin can occur through interactions with NPC proteins (Gozalo et al. 2020; Iglesias et al. 2020; Sarkar et al. 2023). Interestingly, we also identified that three other "peripheral" hits from our screen (Reptin, Pontin, and CG4557) copurified with Stwl, suggesting that a Stwl-containing multiprotein complex may be required to facilitate perinuclear positioning of bound loci. At the same time, our discovery of multiple potential perinuclear anchors suggests a high degree of redundancy in the system. One example of this potential redundancy may be the male germline, where Stwl depletion has no effect on GSC maintenance. We therefore speculate that other proteins function in parallel to Stwl outside of the female germline, and these proteins may include other "peripheral" hits identified in our screen [e.g., Jarid2 and Su(var)3-7] or one of the 45 *Drosophila melanogaster* MADF-BESS family members (e.g., Brwl or Hng2) (Shukla et al. 2014, 2018), which are known to function redundantly in other tissues.

In the absence of Stwl, we observed that GSCs undergo substantial changes in chromatin organization at the nuclear envelope, including gaps in the nuclear lamina and decreased electron-dense perinuclear chromatin foci. These phenotypes appear to be linked, since GSCs containing lamin gaps exhibit a stronger reduction in peripherally associated chromatin, while the lamin gap regions also rarely contain NE-associated electron-dense chromatin foci. Interestingly, the lamin gaps are only observed in female GSCs, which are exquisitely sensitive to Stwl loss, and not seen in other cell types lacking Stwl (e.g., cultured cells). In addition, they do not appear to be caused by decreased lamin levels, since ectopic lamin expression in Stwl mutant GSCs does not rescue the gap phenotype. Rather, we speculate that reduced chromatin associations with the nuclear periphery in the absence of Stwl in GSCs could lead to the dissociation and degradation of the lamina, similar to what has been suggested in senescent mammalian cells (Dou et al. 2015). One reason for the decreased perinuclear chromatin association in Stwl-depleted GSCs could be a lack of bridging interactions between chromatin and the nuclear envelope. Since loss of Stwl has been linked to lowered levels of heterochromatin modifications in whole larvae (Yi et al. 2009), another possibility is that peripheral detachment of specific chromatin loci may occur in concert with defects in global genome and/or heterochromatin organization in cells lacking Stwl. For example, a parallel study (Kotb et al. 2024) has identified that Stwl is enriched at the boundaries between active and inactive genomic regions in young ovaries in a manner reminiscent of insulator proteins that demarcate topologically associated domains (TADs) (Oudelaar and Higgs 2021). In the absence of Stwl, they found that the chromatin states of these active–inactive regions are indistinct, which is suggestive of compartment mixing and is associated with gene misexpression. Intriguingly, previous studies have noted that transcriptionally silent lamina-associated domains (LADs) are separated from neighboring active genomic compartments by a sharp border (Guelen et al. 2008; Dixon et al. 2012). In addition, induced expression of peripherally positioned genes and alteration of their chromatin state results in relocalization to the nuclear interior (Chuang et al. 2006; Therizols et al. 2014). Kotb et al. (2024) have further shown that mixing of active and inactive chromatin states at the *Rps19b* locus in the absence of Stwl is associated with detachment from the nuclear periphery in nurse cells. Therefore, we postulate that heterochromatin–euchromatin compartment mixing in the absence of Stwl may destabilize heterochromatin domains, perinuclear chromatin anchoring, and the nuclear lamina. Moving forward, it will be of great interest to characterize the *cis*-regulatory sequences and protein–protein interactions that shape 3D genome organization at Stwl target loci in GSCs.

In summary, our HiDRO-based nuclear architecture screen has identified multiple potential chromatin-associated perinuclear anchors in the *Drosophila* genome. Here, we focused on Stwl, which we identified as a factor required for positioning chromatin at the nuclear periphery in female GSCs. Strikingly, we show that this property of Stwl is critical to promote female GSC fate through the anchoring of canonical differentiation genes at the repressive perinuclear subcompartment. Thus, our study makes a significant step toward dissecting causal relationships between the position of a gene, the regulation of its expression, and the effect on cell fate decisions in multiple tissues.

Materials and methods

Drosophila *husbandry and strains*

All flies were raised on standard Bloomington medium at 25°C unless otherwise noted. $Stwl^{RNAi}$ (BDSC35415), $mCherry^{RNAi}$ (BDSC35785), $P\{EPgy2\}stwl^{EY00146}$ (BDSC21350), $bam^{\Delta 86}$ (BDSC5427), bam^{RNAi} (BDSC33631), Lam^{A25} (BDSC25092), and $Nup214^{10444}$ (BDSC12369) were obtained from the Bloomington *Drosophila* Stock Center. $stwl^{LL6470}$ (DGRC141809) was obtained from the Kyoto Stock Center. *nos-GAL4*$^{+VP16}$ (third chromosome) (Van Doren et al. 1998), *bam-GAL4* (Chen and McKearin 2003), and bam^{1} (McKearin and Spradling 1990) have been previously described. *nos-GAL4*$^{+VP16}$ (second chromosome) and *nos-GAL4*$^{-VP16}$; $Gal80^{ts}$ were gifts from Yukiko Yamashita. For inducible knockdown experiments, *nos-GAL4*$^{-VP16}$; $Gal80^{ts}$ flies were crossed to the desired RNAi strain at 18°C. Following eclosion, 1 day old flies were collected and shifted to 29°C to induce RNAi expression.

HiDRO and screen data analysis

HiDRO was adapted from Park et al. (2023) for *Drosophila* cells. Plates (384 well; Perkin Elmer 6057300) were seeded with dsRNA by the DRSC screening core at Harvard University. Kc167 cells were resuspended at a concentration of 1×10^6 cells/mL in serum-free Schneider's S2 media (Thermo Fisher R69007), seeded onto 384 well plates at a volume of 10 µL per well using the Matrix WellMate (Thermo Fisher), and then spun down at 1200 rpm for

2 min. Unless otherwise indicated, spins were done at this setting, and pipetting was performed by the WellMate. Plates were allowed to incubate for 30 min at 25°C for dsRNA uptake before being seeded with 30 µL of serum-containing media. Cells were allowed to grow for 4 days. To fix the cells, cells were first washed with 1× PBS and then fixed in 4% paraformaldehyde in 1× PBS for 5 min, with plates spun right after the addition of the fixative to ensure full contact with the cells. PFA was removed and cells were washed and stored in 1× PBS at 4°C.

For the first day of the FISH protocol, 1× PBS was used to wash the cells prior to the addition of a solution of 50% formamide in 2× SSC and 0.1% Tween-20 (50% FMM/2× SSCT). Plates were spun, incubated for 3 min at 91°C on heat blocks (VWR) and then for 20 min at 60°C, and then allowed to cool to room temperature. Wells were aspirated and then filled manually with a multichannel pipette with 20 µL of hybridization mix containing 50% FMM/2× SSCT and 1 pmol of each probe. Plates were spun and placed on the heat blocks for 20 min at 91°C. Plates were spun one more time before incubating on the hot block overnight at 37°C.

For the second day, plates were washed several times with 2× SSCT to completely remove the hybridization mix from wells. Next, plates were incubated twice with 2× SSCT prewarmed for 5 min at 60°C. Plates were then incubated for 5 min with room temperature 2× SSCT, with the last wash containing 1 µg/mL Hoechst 33342. Next, plates were incubated twice for 15 min with room temperature 2× SSC prior to the addition of imaging buffer containing 2× SSC, 10% glucose, 10 mM Tris-HCl, 0.1 mg/mL catalase, and 0.37 mg/mL glucose oxidase.

Plates were imaged within 5 days of the FISH protocol on the Yokogawa CV7000 at the National Cancer Institute High-Throughput Imaging Facility (HiTIF) with the 60× objective and 2 pixel × 2 pixel binning to achieve a resolution of 0.217 µm per pixel. Ten fields were imaged per condition, with *Z*-stacks consisting of 21 slices at 0.5 µm intervals imaged and maximum-projected for 2D analysis.

Images from HiDRO plates were segmented and measured using CellProfiler v3.1.8 (McQuin et al. 2018). Both nuclei and FISH foci were identified using the "global" thresholding strategy and the "Otsu" method. All metrics from the "MeasureObjectSizeShape" module were exported and processed as follows. First, measurements from individual nuclei were summarized by determining the minimum distance of spots to the nuclear periphery, the minimum distance between spots, and the average eccentricity value for each spot. Next, data from all the nuclei per well were aggregated by averaging, and *z*-scores were calculated by comparing the well average to the distribution of values of all wells of the same plate. In order for a gene to be considered a hit, at least two replicates of the same dsRNA treatment for that gene had to surpass an absolute *z*-score cutoff of ≥1.5.

dsRNA production

The following primers were used to both amplify the gene of interest from genomic DNA and add T7 adapters: LacZ (forward: TAATACGACTCACTATAGGGCTGGCGTAATAGCGAAGAGG; reverse: TAATACGACTCACTATAGGGCATTAAAGCGAGTGGCAACA) and Stwl (forward: TAATACGACTCACTATAGGGAGAAGTAGTGTCGCTGCC; reverse: TAATACGACTCACTATAGGGAAAAATCGTCCCAAGACA). The resulting PCR products were purified using a NucleoSpin gel and PCR clean-up kit (Macherey-Nagel). dsRNA was generated using the MEGAscript T7 kit (Invitrogen) and purified using the RNeasy kit (Qiagen). dsRNAs were heated for 30 min to 65°C and then cooled slowly to room temperature to renature dsRNA.

Cell culture and knockdowns

Kc167 cells were obtained from the *Drosophila* Genome Resource Center (DGRC). Cells were grown at 25°C in Schneider's medium supplemented with 10% FBS. Cultures were split twice per week at a 1:4 ratio. For knockdowns, 4×10^6 cells were incubated with 40 µg of dsRNA in 1 mL of serum-free medium for 30 min in each well of a 6 well plate. After incubation, 3 mL of complete medium was added to the cells. Cells were cultured for 4 days. Control cells were treated with dsRNA targeting LacZ.

qPCR

RNA was extracted from cells using the RNeasy kit (Qiagen) and converted to cDNA using the Maxima reverse transcriptase kit (Thermo Scientific). qPCR was run using PowerUp SYBR Green master mix (Applied Biosystems). Genes of interest were compared with the geometric mean of three housekeeping genes (Aldh7A1, P5CS, and Ssadh). Primers used are listed in Table 1.

Table 1. Primers used in this study

Target	Forward sequence	Reverse sequence	Reference
Aldh7A1	ATCCCGGAACTGGTCAACC	CCAGCCCGATGGTATGCTC	DRSC: PP22342
P5CS	AAAAGGCGCATCCAACCTTCA	GACTGCACTGCCCAACTTGA	DRSC: PP8530
Ssadh	CGCAGGAGATAGCCGAGATAA	TGCAAACCACTCGACGAAGG	DRSC: PP20828
Stwl 1	GCCTCTGAGGTGAACCTGATG	GTCCCAGGCGTTCTCACTC	DRSC: PP9552
Stwl 2	GTTGCCTCCGAAGTTGGAGAG	GCGGGTATAGTCATTTCGCAG	DRSC: PP22368
Lamin	CTTAACGAAGACCTGAATGAGGC	CGACAGTGTCTCCTGTTCCAG	DRSC: PP30862

Purification of Stonewall for antibody generation

For expression of N-terminal His_6-tagged Stwl in bacteria, the stonewall coding sequence was amplified by PCR and cloned into the XhoI and NcoI sites of the pET28a vector (Novagen). The plasmid was transformed into *Escherichia coli* BL21(DE3) cells (StrataGene), and protein expression was induced with 0.5 mM IPTG for 4 h at 37°C. For protein purification, cells were resuspended in lysis buffer (6 M GndHCl, 0.1 M NaH_2PO_4, 0.01 M Tris-HCl at pH 8.0), followed by incubation for 60 min at room temperature. The lysate was cleared by centrifugation at 12,000*g* for 30 min at room temperature and added to Ni-NTA agarose beads (Qiagen) equilibrated in lysis buffer. After incubation for 1 h at room temperature, beads were washed once with lysis buffer and twice with wash buffer (8 M urea, 0.1 M NaH_2PO_4, 0.01 M Tris-HCl at pH 6.3). His_6-Stwl was eluted with wash buffer adjusted to pH 4.5 and rebuffered to 1× PBS by dialysis. Antibodies were produced in rabbits and affinity-purified using the recombinant antigen at ProteoGenix.

Generation of Stwl knockout alleles

Stwl knockout (KO) alleles (replacement of protein-coding sequence by a DsRed cassette) were generated using CRISPR-mediated homology-directed repair. Briefly, 1000 bp from the 3′ UTR and 785 bp from the 5′ UTR of Stwl were cloned into a vector (pBSK-attB-DsRed-attB) flanked by a 3XP3-driven DsRed cassette. This plasmid was coinjected along with two gRNA-expressing plasmids (pU6-Bbs1-ChiRNA containing gRNA1: GATCCACTG GCTCTCGCTTA and gRNA2: GCATCAGGTTCACCT CAGAGG) in embryos from the *nos-Cas9* strain (second chromosome, BDSC78781) by BestGene, Inc. Transformants were selected based on DsRed expression, and proper integration into the *stwl* locus was verified by PCR. Two independent and validated *stwl* KO alleles ($stwl^{KO4}$ and $stwl^{KO7}$) were used in our experiments.

Fertility assays

For male fertility assays, two *yw* virgin females were crossed to a single tester male in a vial and allowed to mate for 1 week. Subsequently, the tester male was transferred to a new vial with two *yw* virgin females for the next week and so on. For each vial, the number of resulting progenies (F1) was counted until 20 days after setup. Female fertility assays were performed in a similar manner except that a single tester female was crossed to two ~1 day old *yw* males. At least eight replicate crosses were set up for each genotype. Any vials that contained deceased parent flies were omitted from the analyses.

Immunofluorescence staining and microscopy

For cultured cells, Kc167 cells were settled onto poly-L-lysine-coated glass slides at a concentration of 1×10^6 cells/mL for 2 h. Cells were then fixed to the slide for 10 min with 4% formaldehyde in PBS-Triton (1× PBS with 0.01% Triton X-100) at room temperature and stored in PBS at 4°C until use. For the Stwl localization experiment, slides were instead fixed by methanol fixation. After settling cells onto slides for 2 h as above, the slides were dipped into ice-cold PBST (1× PBS with 0.02% Tween-20), incubated in cold methanol for 10 min at −20°C, and stored in PBS at 4°C until use. Cells were permeabilized in 1% Triton-PBS for 15 min and washed three times for 5 min each in PBST (1× PBS with 0.02% Tween-20). Slides were then blocked with BSA-PBST (1× PBS with 0.02% Tween-20 and 2% BSA) for 30 min with nutation. Primary antibodies were diluted in BSA-PBST and applied to the sample, and coverslips were sealed with rubber cement. Slides were incubated overnight at 4°C. The following day, slides were washed three times for 5 min each with PBST. Secondary antibodies were diluted in BSA-PBST, applied to samples, sealed with rubber cement, and incubated for 2 h at room temperature while protected from light. Slides were washed three times for 5 min each with PBST. Slides were incubated with Hoescht (1:10,000 in 2× PBS) for 5 min to stain DNA. Slides were then mounted using SlowFade Gold (Invitrogen).

For formaldehyde fixation and staining of *Drosophila* tissues, three to four ovaries or five to seven testes per sample were dissected in 1× PBS and fixed in 4% EM-grade paraformaldehyde (PFA) for 20 min at room temperature on a nutator. Fixed samples were washed three times using 1× PBS containing 0.1% Triton-X (PBS-T) for 15 min each and blocked using 3% BSA in 1× PBS-T for 30 min. Primary antibodies were diluted in 3% BSA in 1× PBS-T block and added to the samples for overnight incubation at 4°C. On day 2, samples were washed as above and incubated overnight at 4°C with secondary antibodies diluted in 3% BSA in 1× PBS-T. On day 3, samples were washed as above and mounted with VectaShield plus DAPI (Vector Laboratories). For methanol fixation and staining, three to four ovaries were dissected in 1× PBS and fixed in ice-cold 100% methanol for 10 min at −20°C. Following fixation, ovaries were washed and stained as above. The following primary antibodies were used in this study: rabbit anti-Stwl A2 (raised against full-length Stwl), mouse anti-Hts (1B1; 1:20; Developmental Studies Hybridoma Bank [DSHB]), rat anti-Vasa (1:100; DSHB), mouse anti-Lamin Dm0 (ADL84.12; 1:400; DSHB), mouse anti-Lamin C (LC28.26; 1:100; DSHB), mouse anti-Bam (1:50; DSHB), mouse anti-mAb414 (1:100; Abcam ab24609), rat anti-dCENP-A for Kc167 cells (1:100; Active Motif AB_2793749), rabbit anti-dCENP-A for ovaries (1:200; Active Motif AB_2793320), and mouse anti-H3K9me2 (1:100; Abcam ab1220). Rabbit anti-Vasa (1:1000) was a gift from Prashanth Rangan. Guinea pig anti-Lamin Dm0, guinea pig anti-LBR, and guinea pig anti-Otefin were gifts from Georg Krohne. All fluorescence microscopy images were acquired using a Leica TCS SP8 confocal microscope with 63× oil-immersion objectives (NA = 1.4). *Z*-stacks were acquired with a slice thickness of 0.30 μm for the FISH experiments and 0.50 μm for all other experiments.

Immunofluorescence quantification and localization in Kc167 cells

IF images were analyzed using the ImageJ extension Tango (Ollion et al. 2013). Stwl and lamin IF intensity was calculated for each nucleus using the integrated density function. For peripheral localization, images from methanol-fixed IF samples were used. Nuclei were divided into five equal-volume shells using the shell analysis feature. The fractions of signal in the outer four shells were combined to create the peripheral compartment, while the inner shell constituted the center compartment. The average peripheral to center ratio was calculated across three replicates.

Immunofluorescence quantification in ovaries

For quantification of FG Nup intensities and Lamin intensities at the NE, a line was drawn per GSC/CB that intersected the NE at a normal (ungapped) NE region and at a lamin gap NE region with elevated FG Nup signal. The pixel intensity for individual channels at the two intersecting points was estimated using Lecia LAS X software and then plotted as a ratio of the pixel intensity at the lamin gap NE over the pixel intensity at the normal NE for both Lamin and FG Nups. For quantification of Stwl protein expression, we generated regions of interest (ROIs) on a single slice of a germarium, which spanned the entire nuclear area for GSCs, CBs, and cells from region 2a/2b using Fiji. The average pixel intensity of Stwl from each ROI was normalized to the average Stwl pixel intensity from a "reference GSC" for each germarium. Cells from each germarium were normalized to their own reference GSC to minimize variation due to technical reasons.

IF-Oligopaint DNA FISH

For *Drosophila* ovaries, whole-mount tissue immunofluorescence was performed as mentioned above. Subsequently, samples were postfixed with 4% PFA for 50 min and washed three times for 5 min each in 2× SSC containing 0.1% Tween-20 (2× SSC-T). Samples were then washed in 2× SSC-T with increasing formamide concentrations (20%, 40%, and 50%) for 10 min each followed by a final 10 min wash in 50% formamide. Next, samples in 50% formamide plus 2× SSC-T were transferred to a PCR tube and incubated for 4 h at 37°C, 3 min at 92°C, and 20 min at 60°C. After this step, excess formamide solution was removed, and the hybridization mix (20–40 pmol per probe; 36 µL of probe buffer plus 1 µL of RNase A) was added to the ovaries. Samples were denatured for 3 min at 91°C followed by overnight incubation at 37°C in the dark. Following hybridization, samples were first rinsed with 50% formamide plus 2× SSC-T and then washed twice for 30 min each at 37°C. Next, samples were washed once with 20% formamide plus 2× SSC-T for 10 min at room temperature, washed four times with 2× SSC-T for 3 min each, and then mounted with VectaShield plus DAPI. Oligopaints targeting a 100 kb region on chromosome 2R: 23,799,747–23,900,018 were synthesized for *bgcn* locus DNA FISH. Oligopaints were also synthesized for 100 kb regions centered on *Gapdh1*, *ord*, and *Smr*. On a single slice, the shortest distance from the FISH focus to the nuclear periphery (marked by Vasa) was identified visually and measured using the line tool in LAS X Leica software to estimate the NE–focus distances.

RNA FISH

RNA FISH in ovaries was performed using the Stellaris RNA FISH protocol for imaginal discs with minor modifications. Briefly, three to four ovaries were dissected in ice-cold RNase-free 1× PBS and fixed in 4% PFA in 1× PBS for 30 min on a nutator with gentle shaking. Following fixation, samples were washed three times with RNase-free 1× PBS for 5 min each and incubated with 1 mL of 100% ethanol overnight at 4°C on a nutator. The next day, samples were washed with RNase-free wash buffer A (2× SSC, 10% formamide) for 3 min at room temperature and incubated with 100 L of hybridization mix (50–125 nM probes, 2× SSC, 10% dextran sulfate, 1 g/L *E. coli* tRNA, 2 mM vanadyl ribonucleoside complex, 0.5% RNase-free BSA, 10% deionized formamide, nuclease free water) overnight in a humid chamber at 37°C. Following the hybridization, the samples were washed twice with wash buffer A for 30 min each at 37°C and once with wash buffer B for 5 min at 37°C and mounted with VectaShield plus DAPI. *bgcn* RNA FISH probes were designed using the Stellaris probe designer (Biosearch Technologies). polyT FISH probes were used to label mRNA and demarcate the nuclear boundary. For quantification of *bgcn* mRNA intensities, we estimated the average pixel intensity of the *bgcn* mRNA signal using ROIs that either encompassed the entire cell area for GSCs/CBs or encompassed the entire cyst area for cells in region 2a/2b. We then normalized these values to the corresponding values obtained for the total mRNA signal (polyT probes) and then normalized these values again to a reference GSC for each germarium.

Transmission electron microscopy

Ovaries were dissected and fixed in freshly prepared fixative (2.5% glutaraldehyde in 0.1 M sodium cacodylate buffer). Fixed ovaries were stored at 4°C until sectioning. TEM was performed at the Center for Microscopy and Image Analysis at the University of Zürich. Image analysis was performed using Maps Viewer or ImageJ. Images were acquired such that each pixel corresponds to 1.7 nm.

RNA extraction from ovaries and RNA sequencing

Briefly, ovaries from 4–5 day old females were dissected in RNase-free 1× PBS and flash-frozen in liquid nitrogen until RNA extraction. RNA extraction for each replicate was performed using 35 ovaries using the RNeasy RNA extraction kit (Qiagen). Samples were treated with DNase after RNA extraction and purified using an RNA purification kit (Promega). RNA concentrations were assessed using

a Nanodrop as well as a Qubit RNA analyzer for sample quality and RIN scores. Samples of sufficient quality (RIN > 9) were subjected to library preparation (Illumina TruSeq mRNA kit) followed by sequencing using Illumina NovaSeq 6000 (single-read, 100 bp) at the Functional Genomics Center Zürich (FGCZ).

RNA sequencing data analysis

On average, we generated 28.3 million reads per sample. The resulting raw reads were cleaned by removing adaptor sequences, low-quality end trimming, and removal of low-quality reads using BBTools v38.18 (https://sourceforge.net/projects/bbmap). The exact commands used for quality control are available on the Methods in Microbiomics webpage (https://methods-in-microbiomics.readthedocs.io/en/latest/preprocessing/preprocessing.html). Transcript abundances were quantified using Salmon v1.10.1 (Patro et al. 2017) and BDGP6.32. Differential gene expression analysis was performed using the Bioconductor R package DESeq2 v1.37.4 (Love et al. 2014). Raw sequencing reads are accessible through GEO series accession number GSE268943.

Stwl CUT&RUN

CUT&RUN was performed as described by Kotb and colleagues (Sarkar et al. 2023). Briefly, 20 pairs of fly ovaries were dissected per replicate and placed on ice in 1× PBS. Each sample was then treated with the permeabilization buffer (50 mL of PBST, 500 µL of Triton-X) for 1 h at room temperature with nutation, followed by a wash with 1 mL of BBT^+ buffer (0.5 g of BSA final 0.5%, 50 mL of PBST) and subsequent removal of the supernatant. Antibody dilutions were prepared in 500 µL of BBT^+ buffer, and the sample was incubated overnight at 4°C. The next day, the sample was washed with PBT^+ buffer and then incubated with pAG-MNase (1:100) in 500 µL of BBT^+ buffer for 4 h at room temperature. For DNA cleavage, the samples were resuspended in 150 µL of $wash^+$ buffer (20 mM HEPES at pH 7.5, 150 mM NaCl, 0.1% BSA, Roche complete EDTA-free tablet plus 0.5 mM spermidine) and incubated for 45 min at 4°C. The reaction was stopped by adding 150 µL of 2× stop buffer (200 mM NaCl, 20 mM EDTA) for 30 min at 37°C. The sample was then centrifuged at 16,000*g* for 5 min, and the supernatant was carefully extracted and transferred to a fresh Eppendorf tube. Two microliters of 10% SDS and 2.5 µL of 20 mg/mL Proteinase K were added to the supernatant, and the mixture was thoroughly mixed using a brief vortexing procedure. Subsequently, the sample was incubated in a water bath for 2 h at 50°C. It is important to note that this can be stopped at this step and the samples can be stored at −20°C. Twenty microliters of AmpureXP bead slurry and 280 µL of MXP buffer (20% PEG8000, 2.5 M NaCl, 10 mM $MgCl_2$) were added to 150 µL of the supernatant and incubated for 15 min at room temperature. Using a magnetic rack, the beads were collected and the supernatant was discarded. While on the magnetic rack, 1 mL of 80% ethanol was added to each tube without disturbing the beads. The sample was then incubated for a minimum of 30 sec, and the ethanol was gently aspirated until all traces of ethanol were removed. The beads were then air-dried for 2 min, resuspended in 10 µL of RNase-free and DNase-free water, and incubated for 2 min at room temperature. The clear solution (containing the liberated DNA) was then transferred to a new Eppendorf tube. The DNA concentration was determined using a dsDNA high-sensitive Qubit assay, and DNA size distribution was analyzed in samples using a fragment analyzer.

CUT&RUN library preparation and data analysis

The NEBNext Ultra II DNA library preparation kit for Illumina (E7645 and E7103) protocol was followed for library preparation. Reads were first evaluated for their quality using FastQC (v0.11.8; RRID: SCR_014583). Reads were trimmed for adaptor sequences using TrimGalore! (v0.6.6; RRID: SCR_011847) and aligned to the dm6 reference genome version for *D. melanogaster* using Bowtie2 (version 2.2.8; RRID: SCR_016368) with parameters -q -I 50 -X 700 --very-sensitive-local --local --no-mixed --no-unal --no-discordant. Binary alignment map (BAM) files were generated with samtools v1.9 and used in downstream analysis. MACS2 v2.1.0 was used to call significant peaks for samples. IgG was used as control to call peaks. Peaks within ENCODE-blacklisted regions and repetitive sequences >100 bases were removed. Coverage tracks were generated from BAM files using the deepTools 3.2.1 bamCoverage function with parameters –normalize using RPKM bin size 10. For genomic annotation, promoters −500 b to +500 bp relative to the TSS were defined according to the *Drosophila* dm6 reference genome version. ChipSeeker (v1.36.0) was used to annotate Stonewall peaks. Stonewall binding motifs were called using the HOMER (v4.10) findMotifsGenome function. Heat maps of genomic regions were generated with the deepTools 3.2.1 computeMatrix and plotHeatmap commands or EnrichedHeatmap (v1.30.0). A PCA plot of histone modifications was generated using the deepTools 3.2.1 multiBigwigSummary and plotPCA functions. Raw sequencing reads are accessible through GEO series accession number GSE250351.

Affinity purification and mass spectrometry

Approximately 1.5×10^8 Kc167 cells were harvested for each replicate and stored at −80°C until further use. For lysis, cells were thawed and resuspended in a buffer containing 50 mM Tris-HCl (pH 7.4), 150 mM NaCl, 0.3 mM $MgCl_2$, 5% glycerol, 0.5% NP40, protease inhibitor cocktail (PIC), 1× PMSF, and benzonase. Lysis was performed using 25 strokes of a type B pestle followed by a 1 h incubation at 4°C. Lysates were centrifuged at 4300*g* for 25 min at 4°C, and the resulting supernatant was transferred into a fresh tube. Protein concentration was estimated using the BCA method. For the affinity purification, lysates with equal protein concentrations were incubated with rabbit IgG (Merck; control) and

50 µg of Stwl antibody overnight at 4°C. The next day, pre-equilibrated magnetic Protein A/G beads (125 µL of slurry/sample) were added to each sample for ~1.5 h at room temperature while rotating. Following this, beads were washed once with lysis buffer and twice with bead wash buffer (50 mM Tris HCl at pH 7.4, 150 mM NaCl). Washed beads with bound protein complexes were subjected to proteolysis by on-bead digestion. Samples were transferred into a 10 kDa molecular weight cutoff spin column (Vivacon 500, Sartorious) according to the FASP protocol (Wiśniewski et al. 2009). Beads in solution were dried, denaturated in 8 M urea, reduced using 5 mM TCEP for 30 min at 37°C, and alkylated using 10 mM iodoacetamide for 30 min at 37°C. Beads were then washed three times with 250 µL of 50 mM ammonium bicarbonate. During the buffer exchange, samples were centrifuged at 10,000*g*. Subsequently, samples were proteolyzed with 0.5 µg of Trypsin (Promega; sequencing grade) for 16 h at 37°C. The proteolysis was quenched with 5% formic acid, and peptides were subjected to C18 cleanup (BioPureSPN Proto 300 C18, The Nest Group) per the manufacturer's procedure. The eluted peptides were then dried using a speedvac and resuspended in 20 µL of 2% acetonitrile and 0.1% formic acid. LC-MS/MS was performed on an Orbitrap Exploris 480 mass spectrometer (Thermo Fisher) coupled to a Vanquish Neo liquid chromatography system (Thermo Fisher). Peptides were separated using a reverse-phase column (75 µm ID × 400 mm new objective, in-house-packed with ReproSil Gold 120 C18, 1.9 µm; Dr. Maisch GmbH) across a 180 min linear gradient from 7% to 50% using buffer A (0.1% [v/v] formic acid) and buffer B (0.1% [v/v] formic acid, 80% [v/v] acetonitrile). Samples were acquired in DDA mode (data-dependent acquisition) with MS1 scan (scan range = 350–1500, R = 60,000, maximum injection time automatic, and AGC target = 100), followed by 30 dependent MS2 scans (scan range = 120–2100, R = 30,000, maximum injection time automatic, and AGC target = 200). Peptides with charge between 2 and 6 were isolated (m/z = 1.4) and fragmented (NCE 28%). Acquired spectra were analyzed using MaxQuant software version 1.5.2.8 against the *Drosophila* proteome reference data set (http://www.uniprot.org, downloaded on January 18, 2021; 22,044 proteins including proteins not reviewed) extended with reverse decoy sequences. The search parameters were set to include specific tryptic peptides, a maximum of two missed cleavages, carbamidomethyl as a static peptide modification, oxidation (M) and deamidation (N-terminal) as variable modifications, and the "match between runs" option. The MS and MS/MS mass tolerance was set to 10 ppm. A false discovery rate of <1% was used at PSM and protein level. Protein abundance was determined from the intensity of the top two unique peptides. Intensity values of proteins identified in all replicates in at least one condition (Stwl pull-down or control pull-down) were median-normalized and imputed using random sampling from a normal distribution generated from 1% lower values. Statistical analysis was performed using unpaired two-sided t-test. Hits identified from the differential analysis between the Stwl pull-down versus the IgG control, with $\log_2$FC > 1 and P-value < 0.05, were considered as interacting proteins. Raw data are accessible through the ProteomeXchange Consortium (PXD046253).

Egg chamber classification and quantification

Ovaries from *bam-Gal4>mCherry*^{RNAi} or *bam-Gal4>Stwl*^{RNAi} females were dissected in 1× PBS followed by the addition of VectaShield containing DAPI. Ovarioles were gently separated and mounted on a glass slide. Egg chamber stages were classified and quantified as described elsewhere (Jia et al. 2016).

Competing interest statement

The authors declare no competing interests.

Acknowledgments

We are indebted to the members of the Jagannathan laboratory, Joyce laboratory, and Rangan laboratory; Gabriel Neurohr; and Tatjana Kleele for their comments on the manuscript. We thank Hugo Stocker for his valuable suggestions throughout the course of the project. We are grateful to Dan Hasson from the Bioinformatics for Next-Generation Sequencing (BiNGS) Core for assistance with the CUT&RUN data analysis, and Shinichi Sunagawa from Eidgenössische Technische Hochschule (ETH) Zürich for providing bioinformatics resources. We thank the Bloomington *Drosophila* Stock Center, Vienna *Drosophila* Resource Center, Berkeley *Drosophila* Genome Project Gene Disruption Project, and FlyBase for reagents and resources. We thank Georg Krohne and Victor Corces for sharing antibodies. We thank the Functional Genomics Center Zurich (FGCZ), the Center for Microscopy and Image Analysis, the Scientific Center for Optical and Electron Microscopy (ScopeM), and the Mass Spectrometry Facility at the Institute of Biochemistry ETH Zürich for technical support. M.J. is supported by a project grant (310030_189131) from the Swiss National Science Foundation. P.R. is funded by grants from the National Institutes of Health (NIH)/National Institute of General Medical Sciences (NIGMS; R01GM111779, RO1GM135628, and R56AG082906). E.F.J. is funded by grants from the NIH/NIGMS (R35GM128903), the NIH/National Institute of Child Health and Human Development (NICHD; R21HD107261), the National Science Foundation (2207050), and the 4D Nucleome Common Fund (U01DA052715 and U01DK127405). U.K. is funded by a project grant (310030_219203) from the Swiss National Science Foundation. A.C. acknowledges support from the Genetics Society of America in the form of a DeLill Nasser Award for Professional Development in Genetics. This work was supported in part by the BiNGS shared resource facility within the Tisch Cancer Institute at the Icahn School of Medicine at Mount Sinai, which is partially supported by NIH grant P30CA196521. This work was also supported in part through the

computational resources and staff expertise provided by Scientific Computing at the Icahn School of Medicine at Mount Sinai and supported by the Clinical and Translational Science Awards (CTSA) grant UL1TR004419 from the National Center for Advancing Translational Sciences. Research reported in this study was also supported by the Office of Research Infrastructure of the NIH under award number S10OD026880.

Author contributions: E.F.J., M.J., A.C., and R.I. conceived the project. A.C., R.I., S.C.N., N.M.K., and J.H. designed and performed most of the experiments, except for Stwl purification, which was performed by C.A. G.U. performed the CUT&RUN data analysis, and A.S. performed the RNA-seq data analysis. AP-MS was performed with the help of F.U., who also analyzed the data. E.F.J., M.J., A.C., and R.I. wrote the manuscript with input from all authors.

References

Ables ET, Drummond-Barbosa D. 2010. The steroid hormone ecdysone functions with intrinsic chromatin remodeling factors to control female germline stem cells in *Drosophila*. *Cell Stem Cell* **7:** 581–592. doi:10.1016/j.stem.2010.10.001

Akhtar W, de Jong J, Pindyurin AV, Pagie L, Meuleman W, de Ridder J, Berns A, Wessels LFA, van Lohuizen M, van Steensel B. 2013. Chromatin position effects assayed by thousands of reporters integrated in parallel. *Cell* **154:** 914–927. doi:10.1016/j.cell.2013.07.018

Akiyama T. 2002. Mutations of *stonewall* disrupt the maintenance of female germline stem cells in *Drosophila melanogaster*. *Dev Growth Differ* **44:** 97–102. doi:10.1046/j.1440-169x.2002.00625.x

Barton LJ, Pinto BS, Wallrath LL, Geyer PK. 2013. The *Drosophila* nuclear lamina protein otefin is required for germline stem cell survival. *Dev Cell* **25:** 645–654. doi:10.1016/j.devcel.2013.05.023

Bhaskar V, Courey AJ. 2002. The MADF-BESS domain factor Dip3 potentiates synergistic activation by Dorsal and Twist. *Gene* **299:** 173–184. doi:10.1016/S0378-1119(02)01058-2

Bian Q, Khanna N, Alvikas J, Belmont AS. 2013. β-Globin *cis*-elements determine differential nuclear targeting through epigenetic modifications. *J Cell Biol* **203:** 767–783. doi:10.1083/jcb.201305027

Chaly N, Munro SB. 1996. Centromeres reposition to the nuclear periphery during L6E9 myogenesis in vitro. *Exp Cell Res* **223:** 274–278. doi:10.1006/excr.1996.0082

Chen D, McKearin DM. 2003. A discrete transcriptional silencer in the *bam* gene determines asymmetric division of the *Drosophila* germline stem cell. *Development* **130:** 1159–1170. doi:10.1242/dev.00325

Chen H, Zheng X, Zheng Y. 2014. Age-associated loss of lamin-B leads to systemic inflammation and gut hyperplasia. *Cell* **159:** 829–843. doi:10.1016/j.cell.2014.10.028

Cheng J, Allgeyer ES, Richens JH, Dzafic E, Palandri A, Lewków B, Sirinakis G, St Johnston D. 2021. A single-molecule localization microscopy method for tissues reveals nonrandom nuclear pore distribution in *Drosophila*. *J Cell Sci* **134:** jcs259570. doi:10.1242/jcs.259570

Chuang C-H, Carpenter AE, Fuchsova B, Johnson T, de Lanerolle P, Belmont AS. 2006. Long-range directional movement of an interphase chromosome site. *Curr Biol* **16:** 825–831. doi:10.1016/j.cub.2006.03.059

Clark KA, McKearin DM. 1996. The *Drosophila stonewall* gene encodes a putative transcription factor essential for germ cell development. *Development* **122:** 937–950. doi:10.1242/dev.122.3.937

Cléard F, Delattre M, Spierer P. 1997. SU(VAR)3-7, a *Drosophila* heterochromatin-associated protein and companion of HP1 in the genomic silencing of position-effect variegation. *EMBO J* **16:** 5280–5288. doi:10.1093/emboj/16.17.5280

Dialynas G, Speese S, Budnik V, Geyer PK, Wallrath LL. 2010. The role of *Drosophila* Lamin C in muscle function and gene expression. *Development* **137:** 3067–3077. doi:10.1242/dev.048231

Dixon JR, Selvaraj S, Yue F, Kim A, Li Y, Shen Y, Hu M, Liu JS, Ren B. 2012. Topological domains in mammalian genomes identified by analysis of chromatin interactions. *Nature* **485:** 376–380. doi:10.1038/nature11082

Dou Z, Xu C, Donahue G, Shimi T, Pan J-A, Zhu J, Ivanov A, Capell BC, Drake AM, Shah PP, et al. 2015. Autophagy mediates degradation of nuclear lamina. *Nature* **527:** 105–109. doi:10.1038/nature15548

Finlan LE, Sproul D, Thomson I, Boyle S, Kerr E, Perry P, Ylstra B, Chubb JR, Bickmore WA. 2008. Recruitment to the nuclear periphery can alter expression of genes in human cells. *PLoS Genet* **4:** e1000039. doi:10.1371/journal.pgen.1000039

Gerstein MB, Lu ZJ, Van Nostrand EL, Cheng C, Arshinoff BI, Liu T, Yip KY, Robilotto R, Rechtsteiner A, Ikegami K, et al. 2010. Integrative analysis of the *Caenorhabditis elegans* genome by the modENCODE project. *Science* **330:** 1775–1787. doi:10.1126/science.1196914

Gonzalez-Sandoval A, Towbin BD, Kalck V, Cabianca DS, Gaidatzis D, Hauer MH, Geng L, Wang L, Yang T, Wang X, et al. 2015. Perinuclear anchoring of H3K9-methylated chromatin stabilizes induced cell fate in *C. elegans* embryos. *Cell* **163:** 1333–1347. doi:10.1016/j.cell.2015.10.066

Gozalo A, Duke A, Lan Y, Pascual-Garcia P, Talamas JA, Nguyen SC, Shah PP, Jain R, Joyce EF, Capelson M. 2020. Core components of the nuclear pore bind distinct states of chromatin and contribute to Polycomb repression. *Mol Cell* **77:** 67–81.e7. doi:10.1016/j.molcel.2019.10.017

Guelen L, Pagie L, Brasset E, Meuleman W, Faza MB, Talhout W, Eussen BH, de Klein A, Wessels L, de Laat W, et al. 2008. Domain organization of human chromosomes revealed by mapping of nuclear lamina interactions. *Nature* **453:** 948–951. doi:10.1038/nature06947

Guerreiro I, Kind J. 2019. Spatial chromatin organization and gene regulation at the nuclear lamina. *Curr Opin Genet Dev* **55:** 19–25. doi:10.1016/j.gde.2019.04.008

Harr JC, Luperchio TR, Wong X, Cohen E, Wheelan SJ, Reddy KL. 2015. Directed targeting of chromatin to the nuclear lamina is mediated by chromatin state and A-type lamins. *J Cell Biol* **208:** 33–52. doi:10.1083/jcb.201405110

Heck BW, Zhang B, Tong X, Pan Z, Deng W-M, Tsai C-C. 2012. The transcriptional corepressor SMRTER influences both notch and ecdysone signaling during *Drosophila* development. *Biol Open* **1:** 182–196. doi:10.1242/bio.2011047

Herz H-M, Mohan M, Garrett AS, Miller C, Casto D, Zhang Y, Seidel C, Haug JS, Florens L, Washburn MP, et al. 2012. Polycomb repressive complex 2-dependent and -independent functions of Jarid2 in transcriptional regulation in *Drosophila*. *Mol Cell Biol* **32:** 1683–1693. doi:10.1128/MCB.06503-11

Hou H, Zhou Z, Wang Y, Wang J, Kallgren SP, Kurchuk T, Miller EA, Chang F, Jia S. 2012. Csi1 links centromeres to the nuclear envelope for centromere clustering. *J Cell Biol* **199:** 735–744. doi:10.1083/jcb.201208001

Iglesias N, Paulo JA, Tatarakis A, Wang X, Edwards AL, Bhanu NV, Garcia BA, Haas W, Gygi SP, Moazed D. 2020. Native chromatin proteomics reveals a role for specific nucleoporins in heterochromatin organization and maintenance. *Mol Cell* **77:** 51–66.e8. doi:10.1016/j.molcel.2019.10.018

Ikegami K, Egelhofer TA, Strome S, Lieb JD. 2010. Caenorhabditis elegans chromosome arms are anchored to the nuclear membrane via discontinuous association with LEM-2. *Genome Biol* **11:** R120. doi:10.1186/gb-2010-11-12-r120

Jia D, Xu Q, Xie Q, Mio W, Deng W-M. 2016. Automatic stage identification of *Drosophila* egg chamber based on DAPI images. *Sci Rep* **6:** 18850. doi:10.1038/srep18850

Joyce EF, Apostolopoulos N, Beliveau BJ, Wu C-t. 2013. Germline progenitors escape the widespread phenomenon of homolog pairing during *Drosophila* development. *PLoS Genet* **9:** e1004013. doi:10.1371/journal.pgen.1004013

Klymenko T, Papp B, Fischle W, Köcher T, Schelder M, Fritsch C, Wild B, Wilm M, Müller J. 2006. A Polycomb group protein complex with sequence-specific DNA-binding and selective methyl-lysine-binding activities. *Genes Dev* **20:** 1110–1122. doi:10.1101/gad.377406

Kohwi M, Lupton JR, Lai S-L, Miller MR, Doe CQ. 2013. Developmentally regulated subnuclear genome reorganization restricts neural progenitor competence in *Drosophila*. *Cell* **152:** 97–108. doi:10.1016/j.cell.2012.11.049

Kotb NM, Ulukaya G, Chavan A, Nguyen SC, Proskauer L, Joyce EF, Hasson D, Jagannathan M, Rangan P. 2024. Genome organization regulates nuclear pore complex formation and promotes differentiation during *Drosophila* oogenesis. *Genes Dev* (this issue). doi:10.1101/gad.351402.123

Kumaran RI, Spector DL. 2008. A genetic locus targeted to the nuclear periphery in living cells maintains its transcriptional competence. *J Cell Biol* **180:** 51–65. doi:10.1083/jcb.200706060

Lavoie CA, Ohlstein B, McKearin DM. 1999. Localization and function of Bam protein require the benign gonial cell neoplasm gene product. *Dev Biol* **212:** 405–413. doi:10.1006/dbio.1999.9346

Li J, Gilmour DS. 2013. Distinct mechanisms of transcriptional pausing orchestrated by GAGA factor and M1BP, a novel transcription factor. *EMBO J* **32:** 1829–1841. doi:10.1038/emboj.2013.111

Li Y, Minor NT, Park JK, McKearin DM, Maines JZ. 2009. Bam and Bgcn antagonize *Nanos*-dependent germ-line stem cell maintenance. *Proc Natl Acad Sci* **106:** 9304–9309. doi:10.1073/pnas.0901452106

Love MI, Huber W, Anders S. 2014. Moderated estimation of fold change and dispersion for RNA-seq data with DESeq2. *Genome Biol* **15:** 550. doi:10.1186/s13059-014-0550-8

Maines JZ, Park JK, Williams M, McKearin DM. 2007. Stonewalling *Drosophila* stem cell differentiation by epigenetic controls. *Development* **134:** 1471–1479. doi:10.1242/dev.02810

Mattout A, Pike BL, Towbin BD, Bank EM, Gonzalez-Sandoval A, Stadler MB, Meister P, Gruenbaum Y, Gasser SM. 2011. An EDMD mutation in *C. elegans* lamin blocks muscle-specific gene relocation and compromises muscle integrity. *Curr Biol* **21:** 1603–1614. doi:10.1016/j.cub.2011.08.030

Mayer R, Brero A, von Hase J, Schroeder T, Cremer T, Dietzel S. 2005. Common themes and cell type specific variations of higher order chromatin arrangements in the mouse. *BMC Cell Biol* **6:** 44. doi:10.1186/1471-2121-6-44

McKearin D, Ohlstein B. 1995. A role for the *Drosophila* bag-of-marbles protein in the differentiation of cystoblasts from germline stem cells. *Development* **121:** 2937–2947. doi:10.1242/dev.121.9.2937

McKearin DM, Spradling AC. 1990. *bag-of-marbles*: a *Drosophila* gene required to initiate both male and female gametogenesis. *Genes Dev* **4:** 2242–2251. doi:10.1101/gad.4.12b.2242

McQuin C, Goodman A, Chernyshev V, Kamentsky L, Cimini BA, Karhohs KW, Doan M, Ding L, Rafelski SM, Thirstrup D, et al. 2018. Cellprofiler 3.0: next-generation image processing for biology. *PLoS Biol* **16:** e2005970. doi:10.1371/journal.pbio.2005970

Meers MP, Bryson TD, Henikoff JG, Henikoff S. 2019. Improved CUT&RUN chromatin profiling tools. *Elife* **8:** e46314. doi:10.7554/eLife.46314

Meister P, Taddei A. 2013. Building silent compartments at the nuclear periphery: a recurrent theme. *Curr Opin Genet Dev* **23:** 96–103. doi:10.1016/j.gde.2012.12.001

Morel V, Schweisguth F. 2000. Repression by suppressor of hairless and activation by Notch are required to define a single row of *single-minded* expressing cells in the *Drosophila* embryo. *Genes Dev* **14:** 377–388. doi:10.1101/gad.14.3.377

Ohlstein B, Lavoie CA, Vef O, Gateff E, McKearin DM. 2000. The *Drosophila* cystoblast differentiation factor, *benign gonial cell neoplasm*, is related to DExH-box proteins and interacts genetically with *bag-of-marbles*. *Genetics* **155:** 1809–1819. doi:10.1093/genetics/155.4.1809

Ollion J, Cochennec J, Loll F, Escudé C, Boudier T. 2013. TANGO: a generic tool for high-throughput 3D image analysis for studying nuclear organization. *Bioinformatics* **29:** 1840–1841. doi:10.1093/bioinformatics/btt276

Oudelaar AM, Higgs DR. 2021. The relationship between genome structure and function. *Nat Rev Genet* **22:** 154–168. doi:10.1038/s41576-020-00303-x

Park DS, Nguyen SC, Isenhart R, Shah PP, Kim W, Barnett RJ, Chandra A, Luppino JM, Harke J, Wai M, et al. 2023. High-throughput oligopaint screen identifies druggable 3D genome regulators. *Nature* **620:** 209–217. doi:10.1038/s41586-023-06340-w

Patro R, Duggal G, Love MI, Irizarry RA, Kingsford C. 2017. Salmon provides fast and bias-aware quantification of transcript expression. *Nat Methods* **14:** 417–419. doi:10.1038/nmeth.4197

Peric-Hupkes D, Meuleman W, Pagie L, Bruggeman SWM, Solovei I, Brugman W, Gräf S, Flicek P, Kerkhoven RM, van Lohuizen M, et al. 2010. Molecular maps of the reorganization of genome-nuclear lamina interactions during differentiation. *Mol Cell* **38:** 603–613. doi:10.1016/j.molcel.2010.03.016

Petrovsky R, Krohne G, Großhans J. 2018. Overexpression of the lamina proteins Lamin and Kugelkern induces specific ultrastructural alterations in the morphology of the nuclear envelope of intestinal stem cells and enterocytes. *Eur J Cell Biol* **97:** 102–113. doi:10.1016/j.ejcb.2018.01.002

Pickersgill H, Kalverda B, de Wit E, Talhout W, Fornerod M, van Steensel B. 2006. Characterization of the *Drosophila* melanogaster genome at the nuclear lamina. *Nat Genet* **38:** 1005–1014. doi:10.1038/ng1852

Poleshko A, Mansfield KM, Burlingame CC, Andrake MD, Shah NR, Katz RA. 2013. The human protein PRR14 tethers heterochromatin to the nuclear lamina during interphase and mitotic exit. *Cell Rep* **5:** 292–301. doi:10.1016/j.celrep.2013.09.024

Reddy KL, Zullo JM, Bertolino E, Singh H. 2008. Transcriptional repression mediated by repositioning of genes to the nuclear lamina. *Nature* **452:** 243–247. doi:10.1038/nature06727

Rohrbaugh M, Clore A, Davis J, Johnson S, Jones B, Jones K, Kim J, Kithuka B, Lunsford K, Mitchell J, et al. 2013. Identification and characterization of proteins involved in nuclear organization using *Drosophila* GFP protein trap lines. *PLoS One* **8:** e53091. doi:10.1371/journal.pone.0053091

Sarkar K, Kotb NM, Lemus A, Martin ET, McCarthy A, Camacho J, Iqbal A, Valm AM, Sammons MA, Rangan P. 2023. A feedback loop between heterochromatin and the nucleopore complex controls germ-cell-to-oocyte transition during *Drosophila* oogenesis. *Dev Cell* **58:** 2580–2593.e6. doi:10.1016/j.devcel.2023.08.014

Shaffer CD, Stephens GE, Thompson BA, Funches L, Bernat JA, Craig CA, Elgin SCR. 2002. Heterochromatin protein 2 (HP2), a partner of HP1 in *Drosophila* heterochromatin. *Proc Natl Acad Sci* **99:** 14332–14337. doi:10.1073/pnas.212458899

Shevelyov YY, Lavrov SA, Mikhaylova LM, Nurminsky ID, Kulathinal RJ, Egorova KS, Rozovsky YM, Nurminsky DI. 2009. The B-type lamin is required for somatic repression of testis-specific gene clusters. *Proc Natl Acad Sci* **106:** 3282–3287. doi:10.1073/pnas.0811933106

Shukla V, Habib F, Kulkarni A, Ratnaparkhi GS. 2014. Gene duplication, lineage-specific expansion, and subfunctionalization in the MADF-BESS family patterns the *Drosophila* wing hinge. *Genetics* **196:** 481–496. doi:10.1534/genetics.113.160531

Shukla V, Dhiman N, Nayak P, Dahanukar N, Deshpande G, Ratnaparkhi GS. 2018. Stonewall and Brickwall: two partially redundant determinants required for the maintenance of female germline in *Drosophila*. *G3* **8:** 2027–2041. doi:10.1534/g3.118.200192

Spierer A, Begeot F, Spierer P, Delattre M. 2008. SU(VAR)3-7 links heterochromatin and dosage compensation in *Drosophila*. *PLoS Genet* **4:** e1000066. doi:10.1371/journal.pgen.1000066

Spradling A, Fuller MT, Braun RE, Yoshida S. 2011. Germline stem cells. *Cold Spring Harb Perspect Biol* **3:** a002642. doi:10.1101/cshperspect.a002642

Szklarczyk D, Franceschini A, Wyder S, Forslund K, Heller D, Huerta-Cepas J, Simonovic M, Roth A, Santos A, Tsafou KP, et al. 2015. STRING v10: protein–protein interaction networks, integrated over the tree of life. *Nucleic Acids Res* **43:** D447–D452. doi:10.1093/nar/gku1003

Tas D, Stickley L, Miozzo F, Koch R, Loncle N, Sabado V, Gnägi B, Nagoshi E. 2018. Parallel roles of transcription factors dFOXO and FER2 in the development and maintenance of dopaminergic neurons. *PLoS Genet* **14:** e1007271. doi:10.1371/journal.pgen.1007271

Therizols P, Illingworth RS, Courilleau C, Boyle S, Wood AJ, Bickmore WA. 2014. Chromatin decondensation is sufficient to alter nuclear organization in embryonic stem cells. *Science* **346:** 1238–1242. doi:10.1126/science.1259587

Towbin BD, González-Aguilera C, Sack R, Gaidatzis D, Kalck V, Meister P, Askjaer P, Gasser SM. 2012. Step-wise methylation of histone H3K9 positions heterochromatin at the nuclear periphery. *Cell* **150:** 934–947. doi:10.1016/j.cell.2012.06.051

Ungricht R, Kutay U. 2017. Mechanisms and functions of nuclear envelope remodelling. *Nat Rev Mol Cell Biol* **18:** 229–245. doi:10.1038/nrm.2016.153

Vallone D, Gondi SB, Whitmore D, Foulkes NS. 2004. E-box function in a *period* gene repressed by light. *Proc Natl Acad Sci* **101:** 4106–4111. doi:10.1073/pnas.0305436101

van Bemmel JG, Pagie L, Braunschweig U, Brugman W, Meuleman W, Kerkhoven RM, van Steensel B. 2010. The insulator protein SU(HW) fine-tunes nuclear lamina interactions of the *Drosophila* genome. *PLoS One* **5:** e15013. doi:10.1371/journal.pone.0015013

Van Doren M, Williamson AL, Lehmann R. 1998. Regulation of zygotic gene expression in *Drosophila* primordial germ cells. *Curr Biol* **8:** 243–246. doi:10.1016/S0960-9822(98)70091-0

van Steensel B, Belmont AS. 2017. Lamina-associated domains: links with chromosome architecture, heterochromatin, and gene repression. *Cell* **169:** 780–791. doi:10.1016/j.cell.2017.04.022

Wiśniewski JR, Zougman A, Nagaraj N, Mann M. 2009. Universal sample preparation method for proteome analysis. *Nat Methods* **6:** 359–362. doi:10.1038/nmeth.1322

Xie W, Chojnowski A, Boudier T, Lim JSY, Ahmed S, Ser Z, Stewart C, Burke B. 2016. A-type lamins form distinct filamentous networks with differential nuclear pore complex associations. *Curr Biol* **26:** 2651–2658. doi:10.1016/j.cub.2016.07.049

Yacobi-Sharon K, Namdar Y, Arama E. 2013. Alternative germ cell death pathway in *Drosophila* involves HtrA2/Omi, lysosomes, and a caspase-9 counterpart. *Dev Cell* **25:** 29–42. doi:10.1016/j.devcel.2013.02.002

Yang X-P, Freeman LA, Knapper CL, Amar MJA, Remaley A, Brewer HB, Santamarina-Fojo S. 2002. The E-box motif in the proximal ABCA1 promoter mediates transcriptional repression of the ABCA1 gene. *J Lipid Res* **43:** 297–306. doi:10.1016/S0022-2275(20)30172-3

Yi X, de Vries HI, Siudeja K, Rana A, Lemstra W, Brunsting JF, Kok RM, Smulders YM, Schaefer M, Dijk F, et al. 2009. Stwl modifies chromatin compaction and is required to maintain DNA integrity in the presence of perturbed DNA replication. *Mol Biol Cell* **20:** 983–994. doi:10.1091/mbc.e08-06-0639

Zinshteyn D, Barbash DA. 2022. Stonewall prevents expression of ectopic genes in the ovary and accumulates at insulator elements in *D. melanogaster*. *PLoS Genet* **18:** e1010110. doi:10.1371/journal.pgen.1010110

Zullo JM, Demarco IA, Piqué-Regi R, Gaffney DJ, Epstein CB, Spooner CJ, Luperchio TR, Bernstein BE, Pritchard JK, Reddy KL, et al. 2012. DNA sequence-dependent compartmentalization and silencing of chromatin at the nuclear lamina. *Cell* **149:** 1474–1487. doi:10.1016/j.cell.2012.04.035